Insights on Hydrocarbon-Generation Microfracturing in Organic-Rich Shales

Mohammed Al Duhailan

SUMMARY

A simple analysis was conducted on the Green River Formation, Uinta Basin, Utah to quantify the relationship between factors controlling hydrocarbon-generation microfracturing in organic-rich shales.

Microfracturing in organic-rich shales due to hydrocarbon generation involves a process of four stages: 1) volume expansion, 2) pressure increase, 3) microfracture initiation, 4) microfracture propagation. The existence of water, the level of richness and brittleness are important factors controlling pressure increase due to volume expansion.

Comparison between two aspect ratios reveals that high aspect ratio, which indicates thin flakes of kerogen, favors horizontal microfracturing while vertical microfracturing is favored when aspect ratio is not high enough. This suggests that the geometric shape of the kerogen controls hydrocarbon-generation microfracturing.

Horizontal propagation of microfractures is favored when the stress ratios product is greater than 1 ($R \times \lambda > 1$). When the ratio of pressure to minimum horizontal stress is greater than 1 ($\kappa > 1$) and the stress ratios product is less than 1, vertical propagation is favored. In this study, the observed horizontal microfractures at low pressures are due to the lack of vertical stress constrain applied in the study- referenced experiment that was conducted on the Green River Formation samples. Conducting pyrolysis experiment that includes the application of different values for vertical stress is recommended.

The study concludes with a suggested sequence that facilitates hydrocarbon-generation microfracturing: 1) thermal maturation of organic-rich shale, 2) conversion of kerogen to bitumen, 3) creation of kerogen nanoporosity, 4) conversion of bitumen to oil, 5) significant expansion of the generated oil volume and increase in pressure, 6) controlled initiation of microfractures by kerogen aspect ratio, and 7) controlled propagation of microfractures by poroelastic behavior.

INTRODUCTION

Substantial volume fractions of kerogen in organic-rich shales transforms to hydrocarbons upon reaching certain thermal maturity levels. During primary migration process within these extremely low-permeability rocks, hydrocarbons are expelled from kerogen causing a volume expansion followed by a significant increase in pressure. Consequently, forces of expulsion are initiated driving hydrocarbons to migrate initially along pressure-induced, bedding-parallel microfractures until reaching near-vertical microfractures (Momper, 1978).

In this paper, insights on factors controlling the increase in pressure, initiation and propagation of microfractures are presented. Emphasis is on organic-rich shales of the Green River Formation, Uinta basin, Utah. The significance of microfractures in organic-rich shales is reviewed followed by highlights on previous studies conducted. Then, the analysis of hydrocarbon-generation microfracturing proceeds.

SIGNIFICANCE OF MICROFRACTURES IN ORGANIC-RICH SHALES

Hydrocarbon flow through matrix is an inadequate explanation for migration of hydrocarbon through these extremely low-permeability rocks. Plug permeabilities are too small to measure. Permeabilities on powdered samples ("GRI method") range from 1 micro to 1 femto Darcy (Cluff et.al., 2007) (Figure 1). Higher permeability pathways through shale seem necessary. A network of microfractures might explain the high deliverability of shales (O'Brien et.al., 1996) (Figure 2).

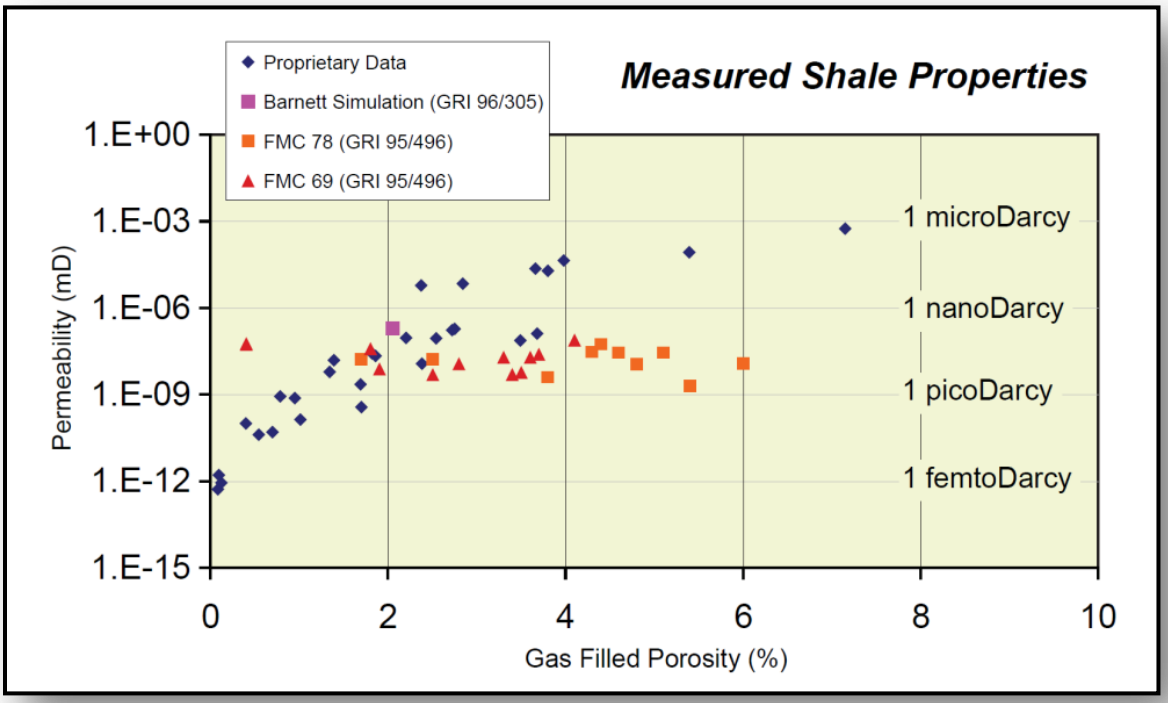

Figure 1: Gas filled porosity versus permeability as measured shale properties using GRI method. Notice the extremely low permeabilities nature of this rock (Cluff et.al., 2007).

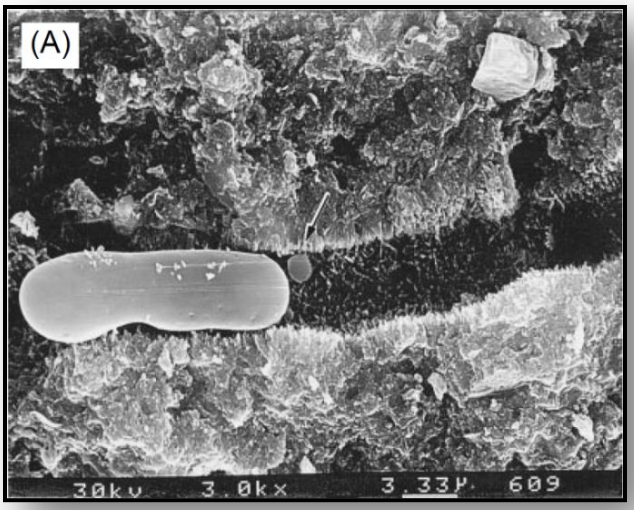

Figure 2: Hydrocarbon droplet morphology seen in scanning electron microscopy within a microfracture (O'Brien et.al., 1996).

Due to the density differences between kerogen and hydrocarbons, fluid pressure increases as a result of a significant volume expansion during the conversion of kerogen to hydrocarbons Figure 3. This volume expansion, which has been invoked as a mechanism to increase pressures, has been documented by several authors. A couple of quotes are documented here:

"At peak-oil-generation, the system pressurizes, partings and microfractures open like the safety valve on a pressure cooker to release the pent-up pressure, and with it, some of the generated fluids. The phenomenon recurs until the generating system runs down." (Momper, 1978).

"The processes of kerogen-to-fluid-oil/gas conversion may cause the generation of abnormally high pressures, facilitating source rock expulsion and migration through fine-grained confining beds through the formation of fractures." (Meissner, 1978).

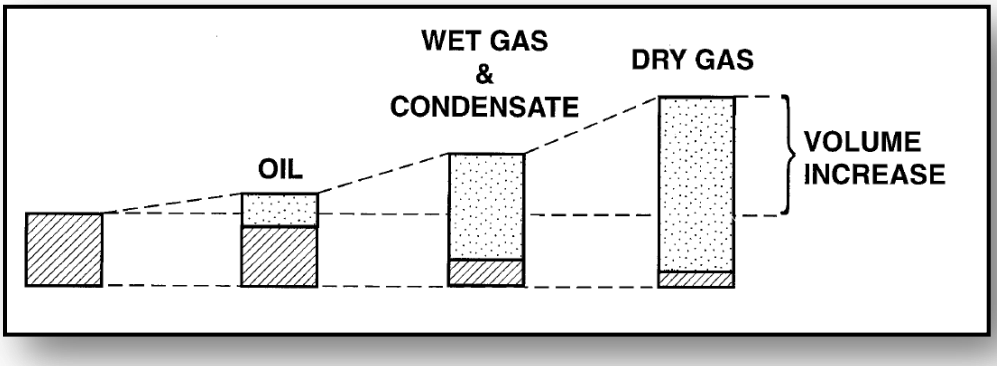

Figure 3: Volume expansion during the conversion of kerogen to oil and gas (modified after Swarbrick and Osborne, 1998, which is modified after Meissner, 1978).

Lewan (1987) preformed a petrographic study of primary petroleum migration in the Woodford shale. He documented that oil expulsion is caused by a net increase in organic components volume which is attributed to the thermal cracking reactions and thermal expansion of the generated oil products. He also pointed out that submicron microfractures are generated to accommodate the net increase in volume (Figure 4).

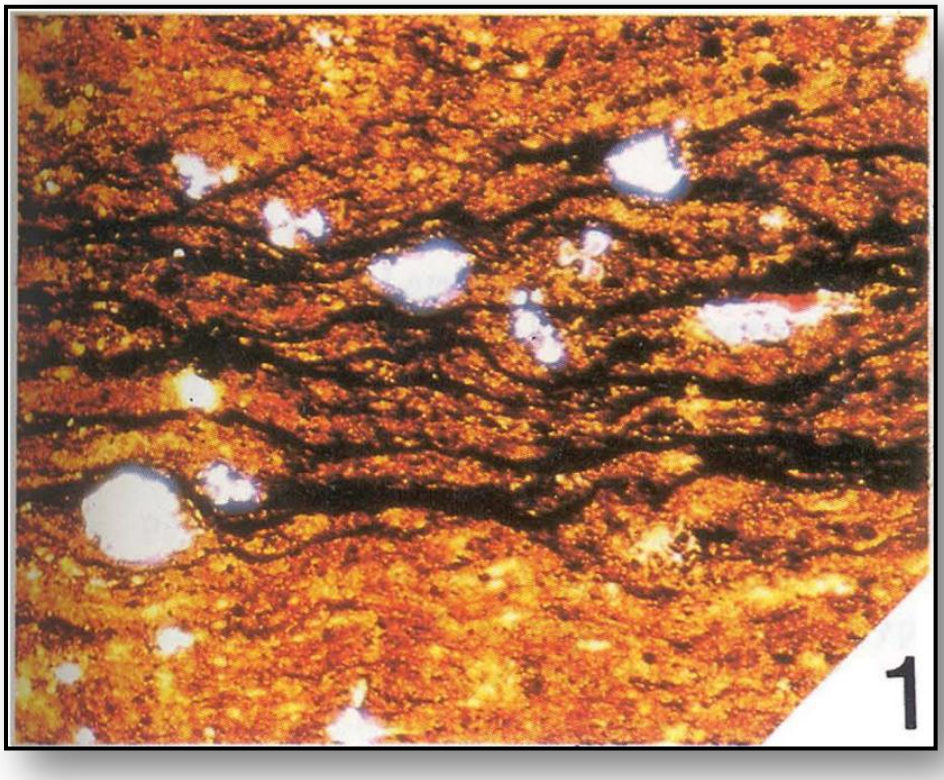

Figure 4: Photomicrograph (Length is 0.88 mm) of Woodford shale sample showing oil in bedding-parallel microfractures (Lewan, 1987).

HYDROCARBON-GENERATION MICROFRACTURING IN ORGANIC-RICH SHALES

The process of microfracturing in organic-rich shales due to hydrocarbon generation involves four stages:

1. Volume expansion
2. Pressure increase
3. Microfracture initiation
4. Microfracture propagation

A study based on quantifying the nature of excess pressure caused by oil generation was undertaken by Berg and Gangi (1999). They derived a simple equation to calculate the pressure change due to oil generation as an application to the Austin Chalk, Texas. With the assumption that nonmineral volume contains only kerogen and water, they observe that the relationship between pressure increase and fraction of converted kerogen differs depending on whether the rock is stiff or compliant.

Initiation of pressure-induced microfractures is explained as a result of local stress concentration around kerogen particles. Özkaya (1988) preformed a simple analysis of stresses around a kerogen particle and pointed out the effect of kerogen shape on the orientation of the microfracture initiated in extremely low permeability organic-rich rocks. Horizontal, layer-parallel microfracture initiation around kerogen particles in finely laminated organic-rich Dunkrik shales, western New York has been observed by Lash and Engelder (2005) (Figure 5). The orientation of flat kerogen particles parallel to the bedding and strength anisotropy of the finely laminated organic-rich Dunkrik shales was proposed to be responsible for horizontal microfracturing.

Utilizing the concept of poroelastic deformation and the role of pressure in microfracturing (e.g. Secor, 1965; Engelder and Lacazette, 1990), conditions that may drive horizontal, layer-parallel crack propagation were highlighted by Lash and Engelder (2005). These horizontal microfractures may connect with vertical microfractures leading to vertical oil migration.

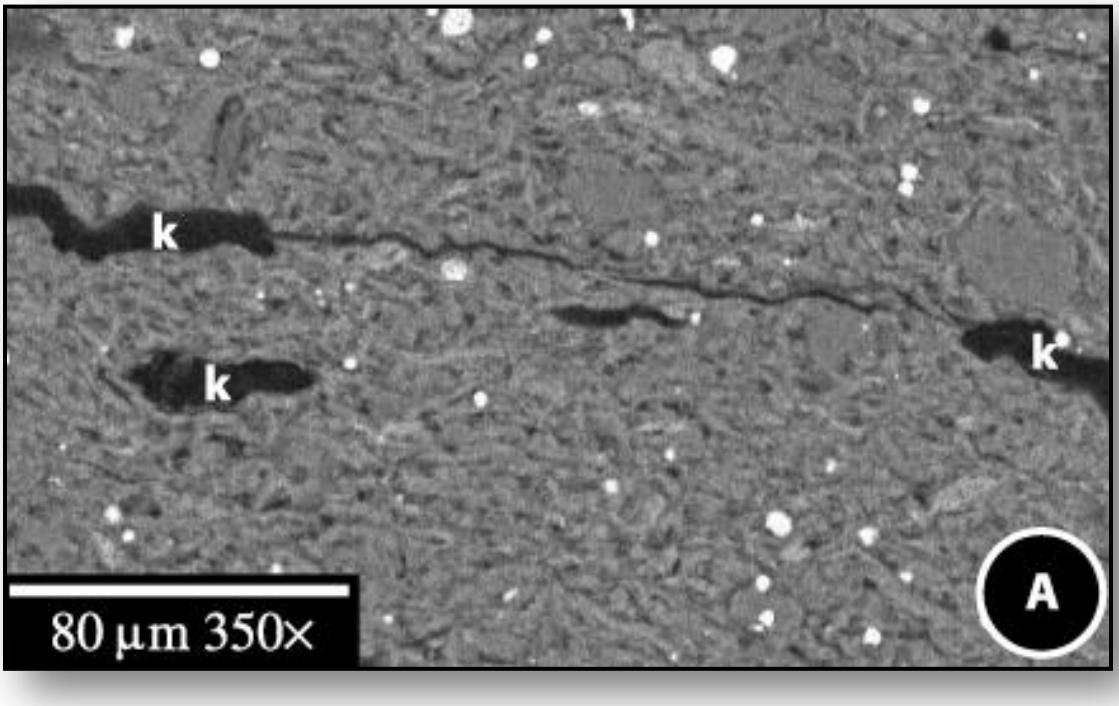

Figure 5: Finely laminated black shale samples showing a microfracture that appear to have originated within (or along the edges of) kerogen (k) particles (Lash and Engelder, 2005).

OBJECTIVE AND APPROACH

Lewan and Roy (2011) conducted hydrous and anhydrous closed-system pyrolysis experiments on samples from the Mahogany zone of the Green River Formation. Extensional microfractures parallel to the bedding fabric were observed as a result of the hydrous pyrolysis. However, there were no microfractures evident from the anhydrous pyrolysis (Figure 6). This has led to the belief on the importance of undertaking this study. The objective is to investigate the factors controlling the increase in pressure due to volume expansion of generated petroleum products, the initiation and propagation of microfractures (Figure 7). The study is proposed to be based on a simple analysis for hydrocarbon-generation microfracturing utilizing the pyrolysis experiments conducted by Lewan and Roy (2011) on samples from the Green River Formation, Uinta basin.

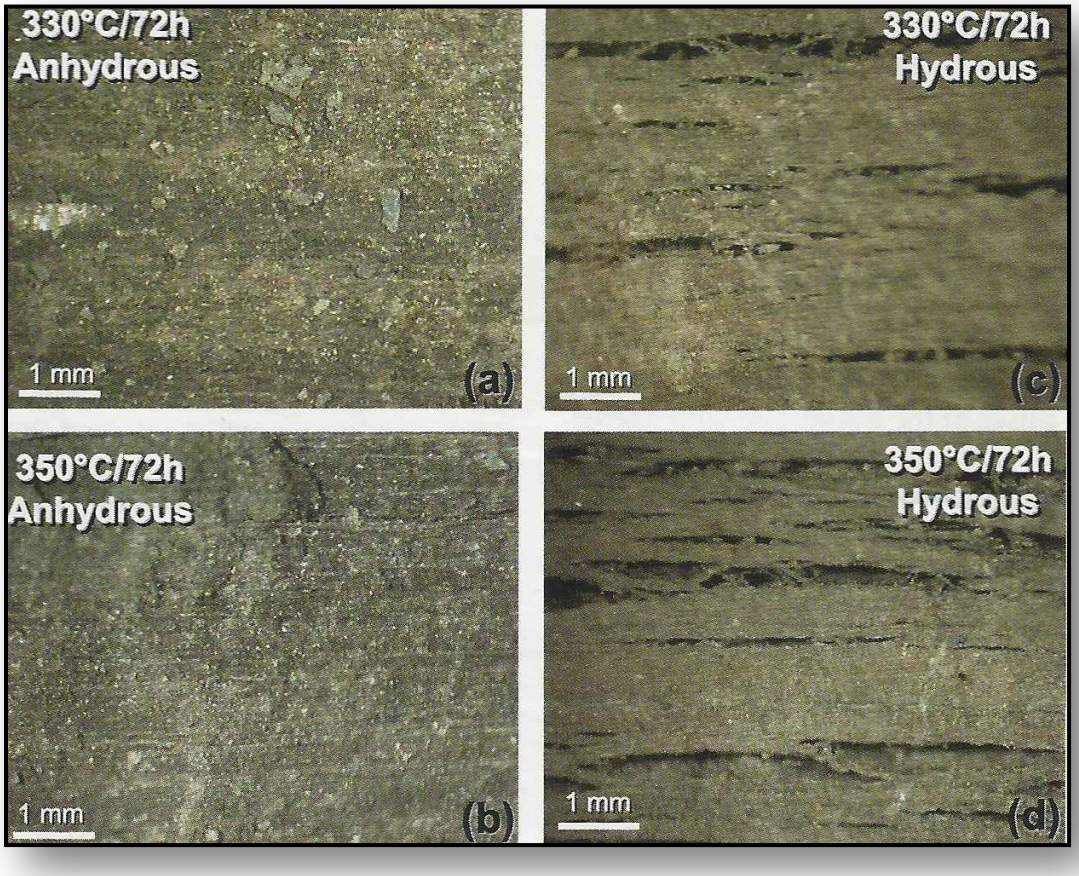

Figure 6: Photomicrographs of rock-chip surfaces perpendicular to bedding fabric of recovered rock from anhydrous and from hydrous experiments (Lewan and Roy, 2011).

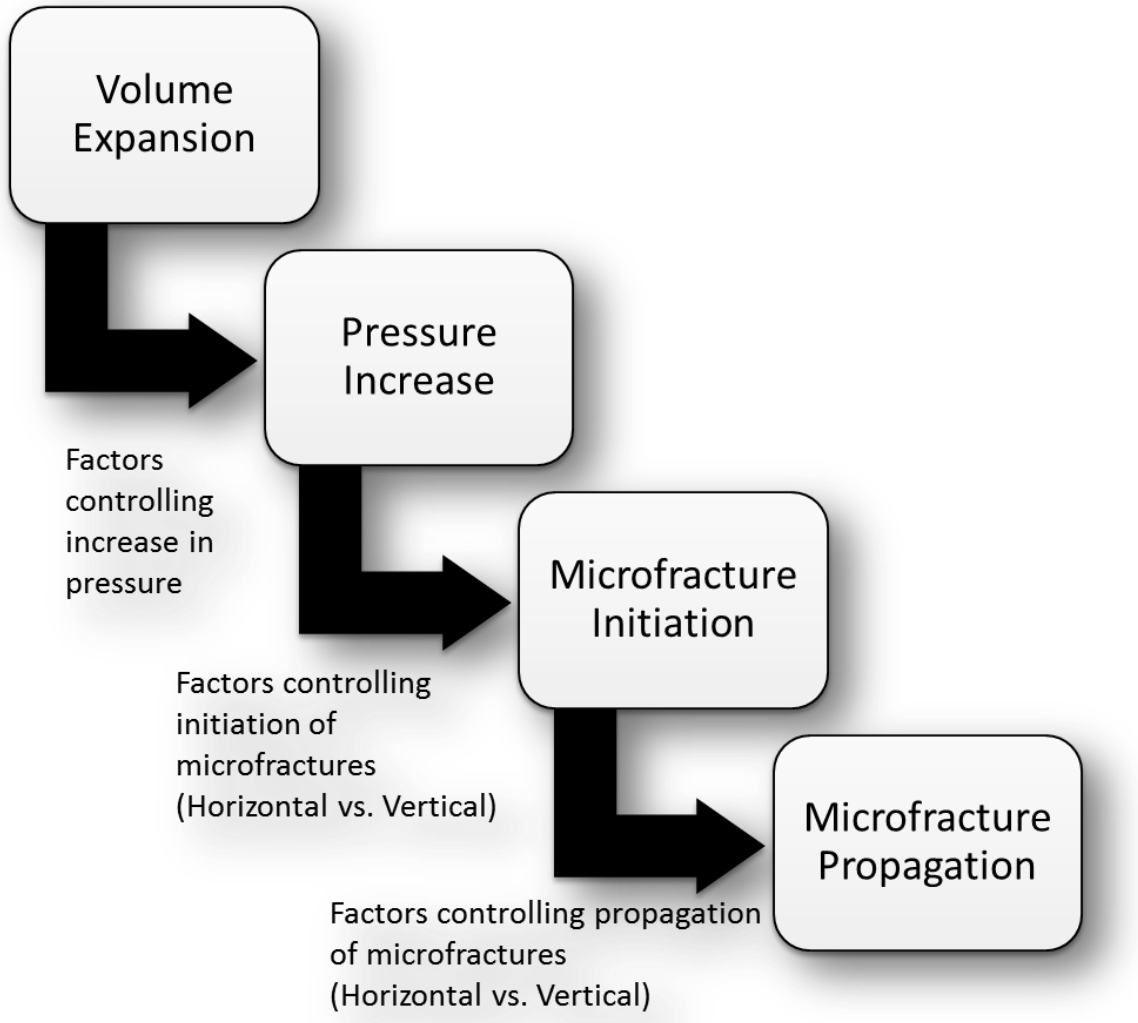

Figure 7: Approach taken for the proposed analysis of hydrocarbon-generation microfracturing

GEOLOGIC BACKGROUND:

As a classic example of a Type-I lacustrine source rock, the Green River Formation hosts the most of the oil shale resources in the United States. A total of 4.29 trillion barrels of oil shale in place is estimated throughout Piceance Creek Basin, Uinta Basin and Green River Basin (Johnson et al., 2011) (Figure 8). The Uinta Basin, which is the focus of this study, is a topographic and structural trough thickly filled with as much as 17,000 ft. of Late Cretaceous and Tertiary age lacustrine and fluvial sedimentary rocks (Fouch et.al., 1994). It is an asymmetrical basin with a steep northern flank. Figure 9 is a cross section showing the structural and stratigraphic configuration of the basin.

The Green River shales are brown, laminated, dolomitic marlstones containing hydrogen-rich kerogen. Figure 10 shows mineral compositions for several mudrocks (Wren, 2011) including a typical mineral composition of the Green River Formation (Dusseault and Loftsson, 1985). The Mahogany zone of Parachute Creek Member encompasses the richest of the Green River Formation (Figure 9). The sedimentologic signature of the Mahogany zone demonstrates offshore open-lacustrine facies preserved under anoxic conditions existed at the lake bottom during deposition (Figure 11). Individual beds can exceed 70 gallons (~32% TOC) of oil per ton of rock (Vanden Berg, 2008) (Figure 12).

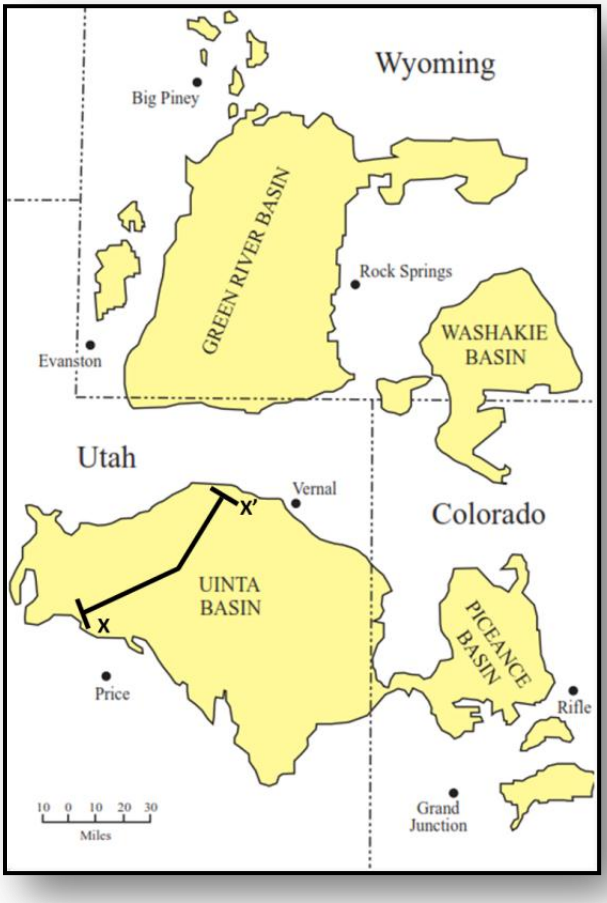

Figure 8: Shale country of the four basins throughout Colorado, Wyoming and Utah (modified after Johnson et al., 2011).

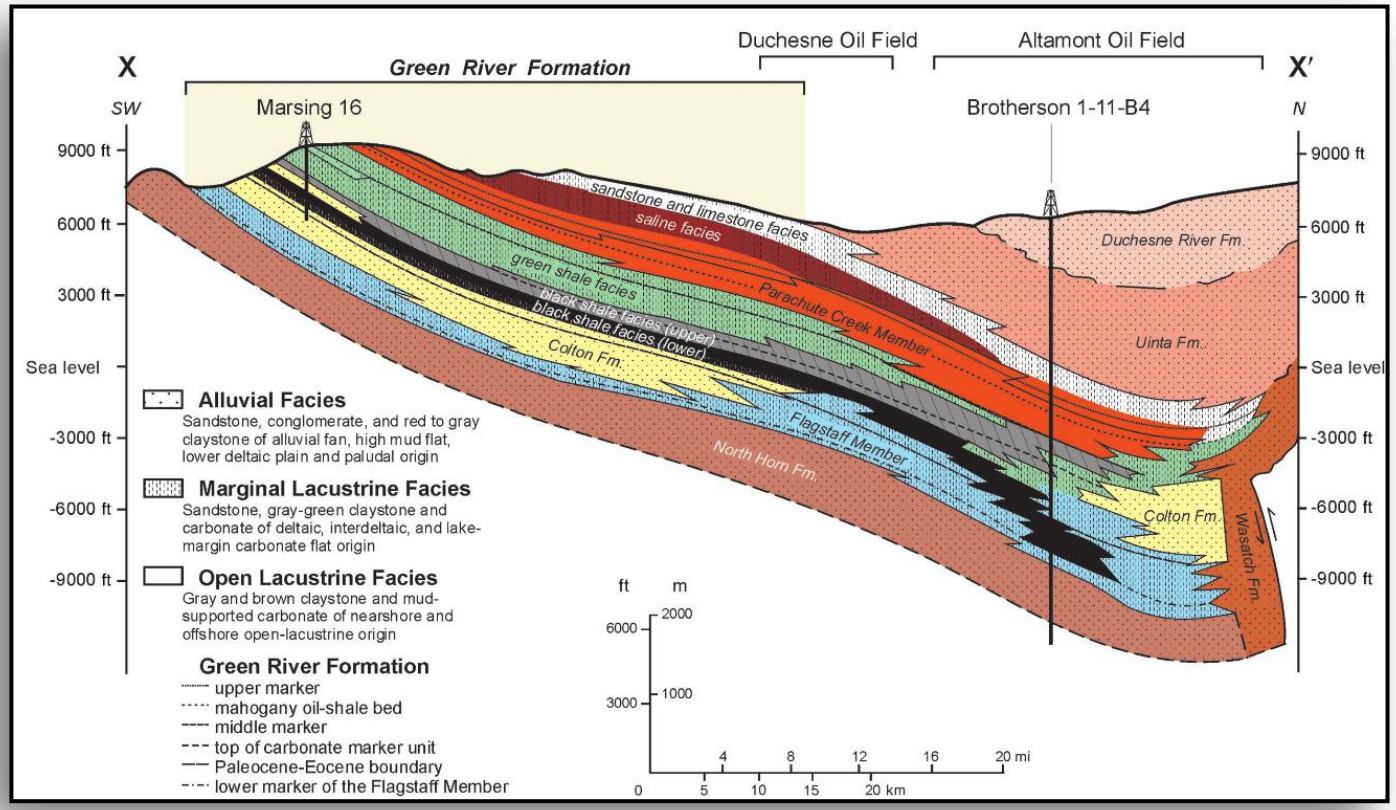

Figure 9: A North-South cross section across the Uinta basin (Ruble et. al., 2001)

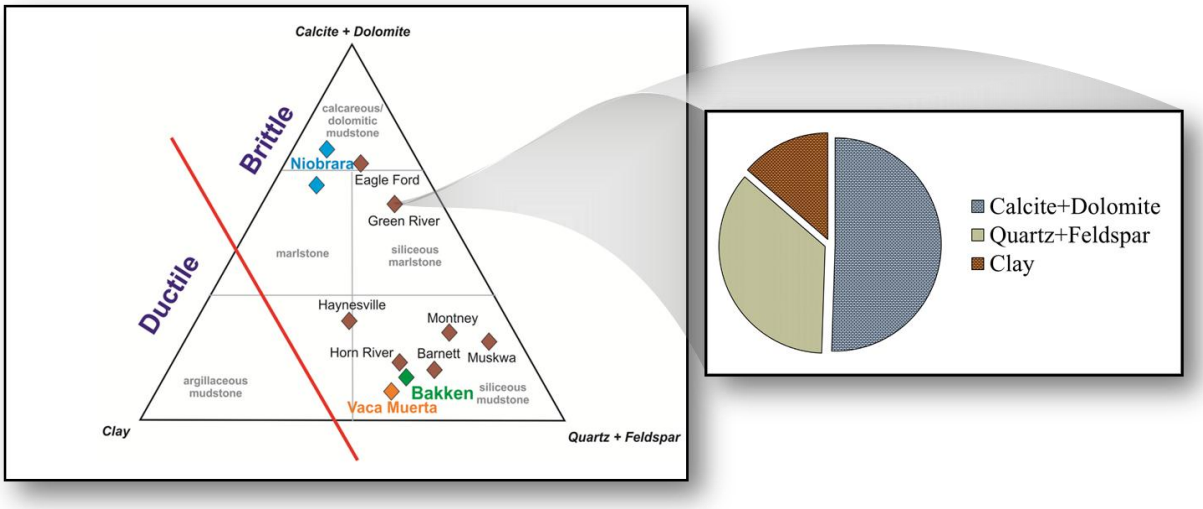

Figure 10: Mineral composition of several mudrocks including a typical mineral composition of the Green River Formation (Wren, 2011) (typical mineral composition data from (Dusseault and Loftsson, 1985). Notice the high percentage of calcite and Dolomite which makes it fall within the brittle mudrocks group.

.

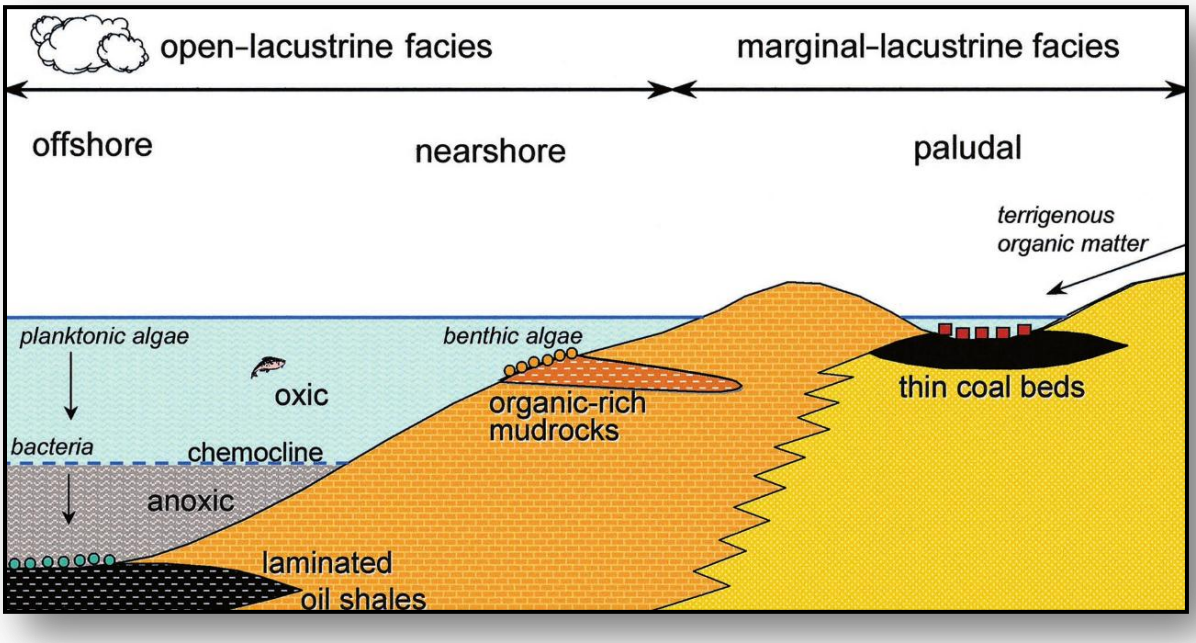

Figure 11: Lacustrine Depositional environment (Ruble et. al., 2001).

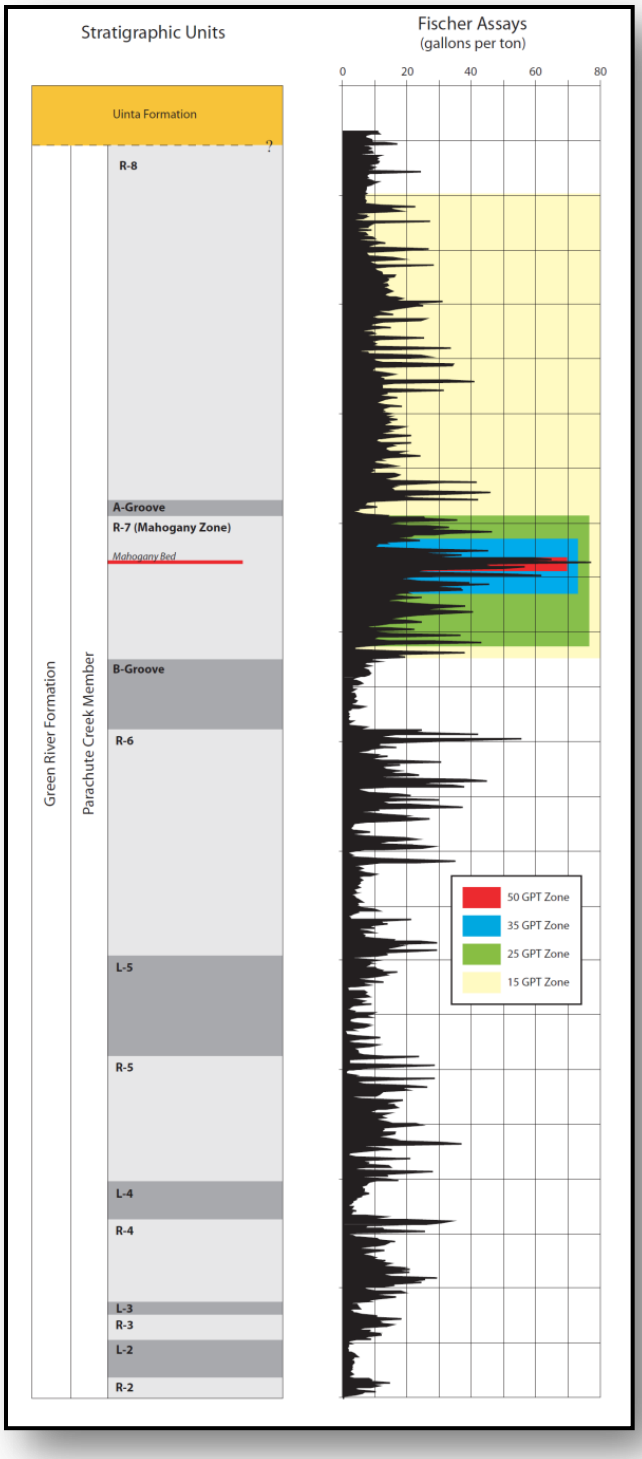

Figure 12: Stratigraphy of the Parachute Creek Member of the upper Green River Formation illustrated by oil-yield plots. “R” refers to a rich oil-shale zone and “L” refers to a lean oil shale zone (Vanden Berg, 2008).

ANALYSIS OF HYDROCARBON-GENERATION MICROFRACTURING:

Samples from the Mahogany zone of the Green River Formation were used by Lewan and Roy (2011) to conduct hydrous and anhydrous closed-system pyrolysis experiments. Hydrous pyrolysis provides insights on stages of petroleum generation: 1) pre-oil generation, 2) initial oil generation, 3) primary oil generation, and 4) post-oil generation (Lewan, 1985) (Figure 13). These stages are reflected by the conversion reactions (kerogen-to-bitumen-to-oil-to-gas). The objective of (Lewan and Roy, 2011) experiment was to examine the role of water during the four stages of petroleum generation. The experiments resulted in 29% more total hydrocarbons generated from the hydrous than the anhydrous experiment. Lewan and Roy (2011) attributed this to the source of hydrogen provided by water, which improves thermal cracking over cross linking. The results showed that the role of water was more significant in bitumen decomposition to oil at 350 ˚C than in kerogen decomposition to bitumen at 330 ˚C. Extensional microfractures parallel to the bedding fabric were observed as a result of volume expansion due to bitumen decomposition to oil in the hydrous pyrolysis. However, there were no microfractures evident from the anhydrous.

Development of Nanoporosity within kerogen particle has been documented by many authors (e.g. Jarvie et.al. 2007; Chalmers and Bustin, 2007; Loucks et.al. 2009) (Figure 14). It has been attributed to the kerogen conversion during thermal maturation. By considering the four stages of petroleum generation, one can postulate that kerogen nanoporosity may be formed during late pre-oil generation to early initial oil generation stage. However, microfractures could be initiated during primary oil generation stage. In (Lewan and Roy, 2011) experiment; there are differences in the generated petroleum products between hydrous and anhydrous experiments. There is more bitumen extract resulted from the anhydrous experiment while there is more generated oil from the hydrous (Figure 15). It implies that only nanoporosity may be found in the samples undergone anhydrous pyrolysis while samples in the hydrous experiment experienced both the development of nanoporosity and microfracturing.

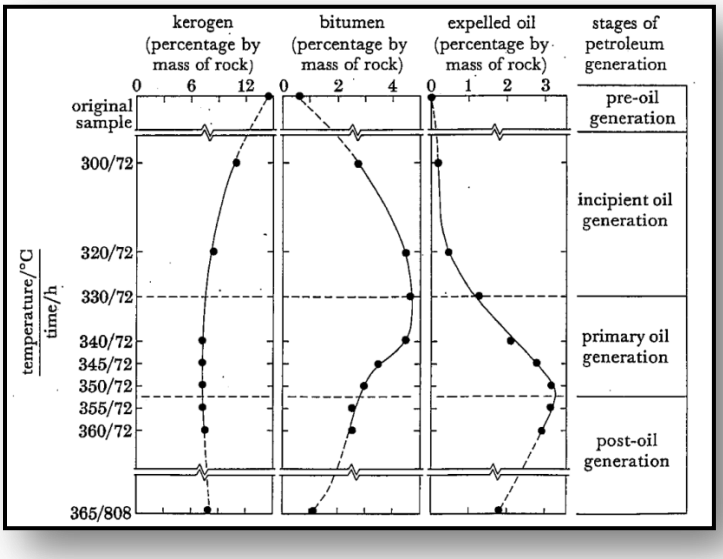

Figure 13: The four stages of petroleum generation (Lewan, 1985).

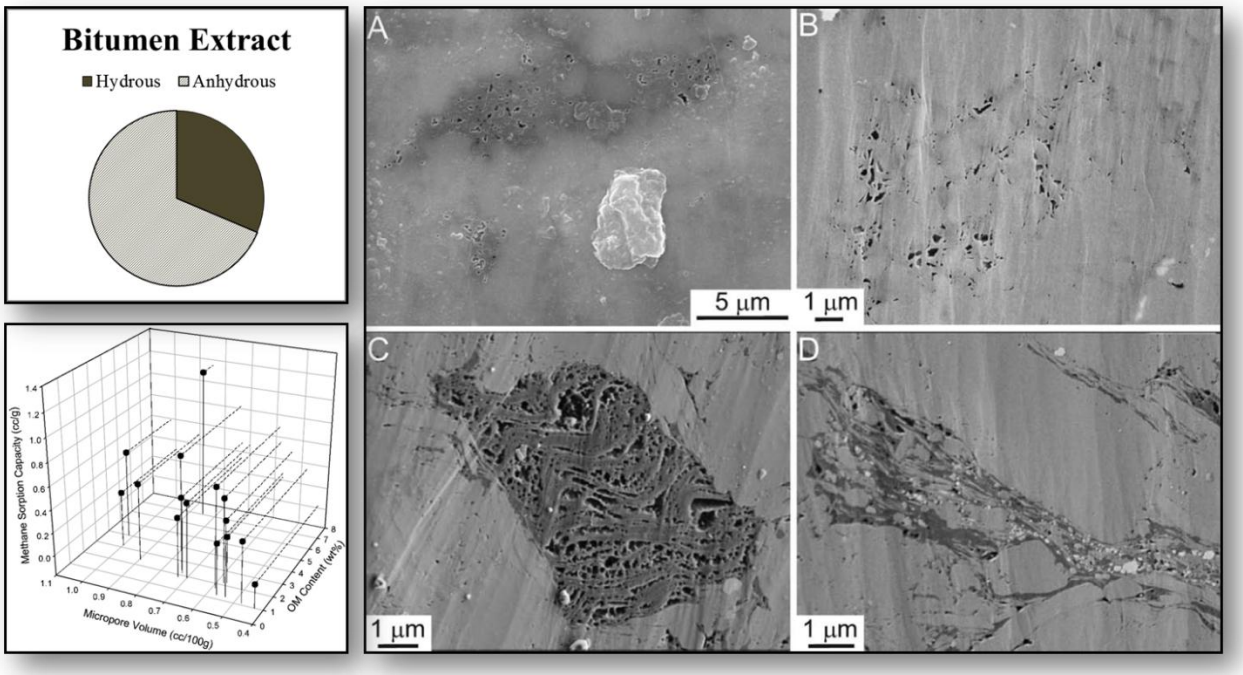

Figure 14: Kerogen nanoporosity (A, B, C, D)(Loucks et.al. 2009). Bottom left figure is the organic content-kerogen nanoporosity relationship (Chalmers and Bustin, 2007).

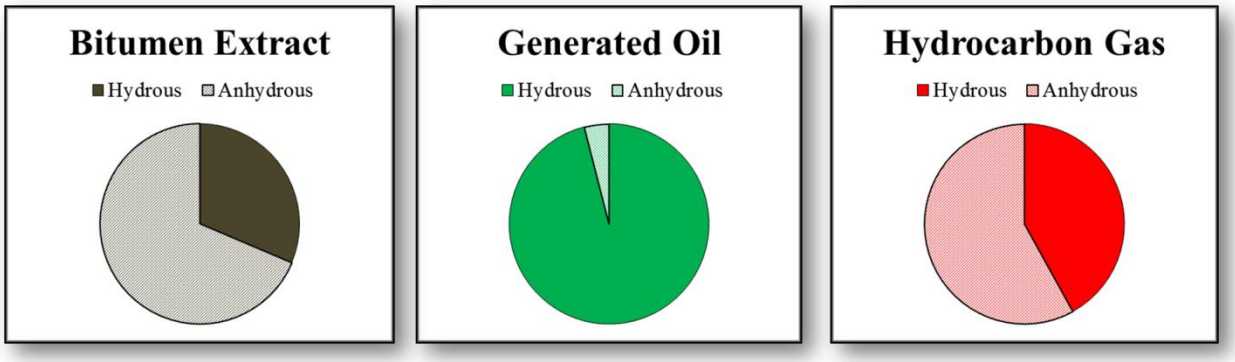

Figure 15: Comparison between (Lewan and Roy, 2011) hydrous and anhydrous pyrolysis according to the generated petroleum products.

The following sections will investigate the factors controlling the pressure increase due to volume expansion, microfracture initiation, and microfracture propagation. Specifically, the role of water, organic richness, brittleness, kerogen aspect ratio, and poroelastic deformation is investigated. Table 1a and b show the input parameters used in the analysis. The data inputs are estimates that are either adapted from actual studies on the Green River Formation or generally known from similar organic-rich shales.

Table 1: Input parameters used in the analysis. a) for the volume expansion and pressure increase and b) for the microfracture initiation and propagation.

(a)

Controlling Factors	Volume Expansion & Pressure Increase					
	Role of Water		Role of Organic Richness		Role of Brittleness	
	Hydroous	Anhydrous	Rich	Lean	Brittle	Ductile
TOC%	15.8	15.8	25	3	15.8	15.8
Converted Fraction	0.2-0.3	0.2-0.3	0.2-0.3	0.2-0.3	0.2-0.3	0.2-0.3
V_w (cm^3)	400	0	400	400	400	400
V_{kr} %	for 15.8% TOC	for 15.8% TOC	for 25% TOC	for 3% TOC	for 15.8% TOC	for 15.8% TOC
V_R	11.8	0	8	50	11.8	11.8
D_{ko}	1.3	1.4	1.2	1.2	1.3	1.3
D_{kr}	-	-	0.44	0.44	-	-
C_w (1/psi)	2.8×10^{-8}	0	2.8×10^{-8}	2.8×10^{-8}	2.8×10^{-8}	2.8×10^{-8}
C_p (1/psi)	3.0×10^{-6}	3.0×10^{-6}	3.0×10^{-6}	3.0×10^{-6}	-	-
C_k (1/psi)	1.0×10^{-5}	1.0×10^{-5}	1.0×10^{-5}	1.0×10^{-5}	1.0×10^{-5}	1.0×10^{-5}
C_o (1/psi)	1.0×10^{-6}	5.0×10^{-4}	1.0×10^{-6}	1.0×10^{-6}	1.0×10^{-6}	1.0×10^{-6}
E (psi)	-	-	-	-	1.0×10^{7}	2.5×10^{6}
v	-	-	-	-	0.1	0.26
Sv (psi)	-	-	-	-	-	-
R	-	-	-	-	-	-
T (psi)	-	-	-	-	-	-
a	-	-	1.3	1.3	-	-
φ %	-	-	10	10	-	-
α	-	-	-	-	-	-

(b)

Controlling Factors	Microfracture Initiation		Microfracture Propagation	
	Role of Aspect Ratio		Role of Poroelastic Deformation	
	Minimum ψ Favoring Horizontal Intitiation	Maximum ψ Favoring Vertical Initiation	Horizontal Propegation	Vertical Propagation
TOC%	15.8	15.8	15.8	15.8
Converted Fraction	0.2-0.3	0.2-0.3	0.2-0.3	0.2-0.3
V_w (cm^3)	400	400	400	400
V_{kr} %	for 15.8% TOC	for 15.8% TOC	for 15.8% TOC	for 15.8% TOC
V_R	11.8	11.8	11.8	11.8
D_{ko}	1.3	1.3	1.3	1.3
D_{kr}	-	-	-	-
C_w (1/psi)	2.8×10^{-8}	2.8×10^{-8}	2.8×10^{-8}	2.8×10^{-8}
C_p (1/psi)	3.0×10^{-6}	3.0×10^{-6}	3.0×10^{-6}	3.0×10^{-6}
C_k (1/psi)	1.0×10^{-5}	1.0×10^{-5}	1.0×10^{-5}	1.0×10^{-5}
C_o (1/psi)	1.0×10^{-6}	1.0×10^{-6}	1.0×10^{-6}	1.0×10^{-6}
E (psi)	-	-	-	-
v	-	-	0.1	0.1
Sv (psi)	200	200	200	600
R	0.7	0.7	-	-
T (psi)	1350	1350	-	-
a	-	-	-	-
φ %	-	-	-	-
α	-	-	1.0	1.0

Volume expansion and pressure increase:

The nature of excess pressure caused by oil generation (Figure 16) was undertaken by Berg and Gangi (1999) with the assumption that:

- Organic-rich shale with very low permeability
- Isotropic stress state
- Compressibility are independent of pressure and temperature
- Volume change due to thermal expansion is neglected
- Non-mineral volume contains only water and kerogen

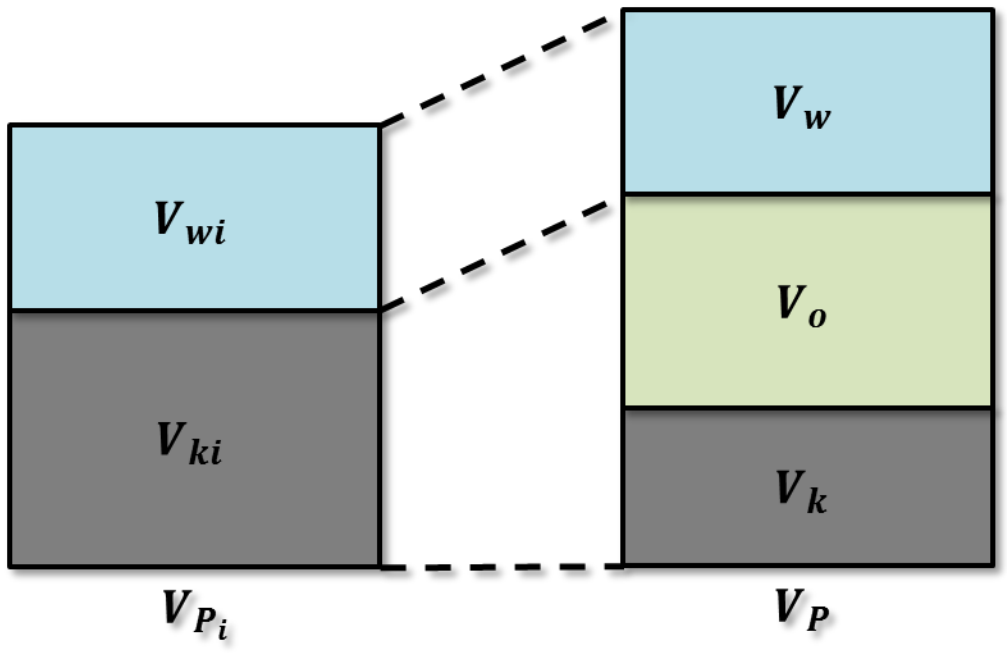

Figure 16: Volume expansion due to kerogen conversion. V_{wi} , V_{ki} , V_{P_i} are the initial water, kerogen volume and pressure increase. V_w , V_k , V_P are the volumes pressure increase after conversion. With F as the converted fraction of kerogen, ($V_k = V_{ki} - FV_{ki}$) and ($V_o = F\left(\frac{\rho_k}{\rho_o}\right)V_{ki}$). ($\frac{\rho_k}{\rho_o}$ is the kerogen to oil density ratio)

Following steps in (Berg and Gangi, 1999) for pressure increase due to volume expansion (Appendix), the following is derived:

$$\Delta P = \frac{F(D_{ko}-1)}{V_R(C_P+C_w)+F(C_k+D_{ko}C_O)+C_P+C_w} \qquad (1)$$

For the role of water, the results show that there is a significant increase in pressure in the hydrous experiment compared to the anhydrous (Figure 17). This is attributed to the low compressibility of water that exists in the hydrous experiment, and lacks in the anhydrous. Also, there are differences in compressibility of the generated oil between the two pyrolysis experiments. Volatile oil has been generated in anhydrous pyrolysis (Lewan and Roy, 2011), which should have higher compressibility than the oil generated in the hydrous pyrolysis. The type of generated petroleum products after kerogen and bitumen conversion is the factor here. Compressibility of the volatile oil is higher than compressibility of the lower molecular weight-oils generated in the hydrous experiment. This resulted in higher pressure increase due to volume expansion in the hydrous experiment.

Hydrous Pyrolysis

V_R	F	D_{ko}	C_w	C_p	C_k	C_o	Δ P
11.80	0.00	1.30	0.000000028	3.00E-06	1.00E-05	1.50E-06	0.00
11.80	0.10	1.30	0.000000028	3.00E-06	1.00E-05	1.50E-06	600.90
11.80	0.20	1.30	0.000000028	3.00E-06	1.00E-05	1.50E-06	1173.70
11.80	0.30	1.30	0.000000028	3.00E-06	1.00E-05	1.50E-06	1720.33
11.80	0.40	1.30	0.000000028	3.00E-06	1.00E-05	1.50E-06	2242.55
11.80	0.50	1.30	0.000000028	3.00E-06	1.00E-05	1.50E-06	2741.96
11.80	0.60	1.30	0.000000028	3.00E-06	1.00E-05	1.50E-06	3220.01
11.80	0.70	1.30	0.000000028	3.00E-06	1.00E-05	1.50E-06	3678.05
11.80	0.80	1.30	0.000000028	3.00E-06	1.00E-05	1.50E-06	4117.32
11.80	0.90	1.30	0.000000028	3.00E-06	1.00E-05	1.50E-06	4538.93
11.80	1.00	1.30	0.000000028	3.00E-06	1.00E-05	1.50E-06	4943.94

Anhydrous Pyrolysis

V_R	F	D_{ko}	C_w	C_p	C_k	C_o	Δ P
0.00	0.00	1.40	2.8E-08	3.00E-06	1.00E-05	5.00E-04	0.00
0.00	0.10	1.40	2.8E-08	3.00E-06	1.00E-05	5.00E-04	476.19
0.00	0.20	1.40	2.8E-08	3.00E-06	1.00E-05	5.00E-04	516.13
0.00	0.30	1.40	2.8E-08	3.00E-06	1.00E-05	5.00E-04	530.97
0.00	0.40	1.40	2.8E-08	3.00E-06	1.00E-05	5.00E-04	538.72
0.00	0.50	1.40	2.8E-08	3.00E-06	1.00E-05	5.00E-04	543.48
0.00	0.60	1.40	2.8E-08	3.00E-06	1.00E-05	5.00E-04	546.70
0.00	0.70	1.40	2.8E-08	3.00E-06	1.00E-05	5.00E-04	549.02
0.00	0.80	1.40	2.8E-08	3.00E-06	1.00E-05	5.00E-04	550.77
0.00	0.90	1.40	2.8E-08	3.00E-06	1.00E-05	5.00E-04	552.15
0.00	1.00	1.40	2.8E-08	3.00E-06	1.00E-05	5.00E-04	553.25

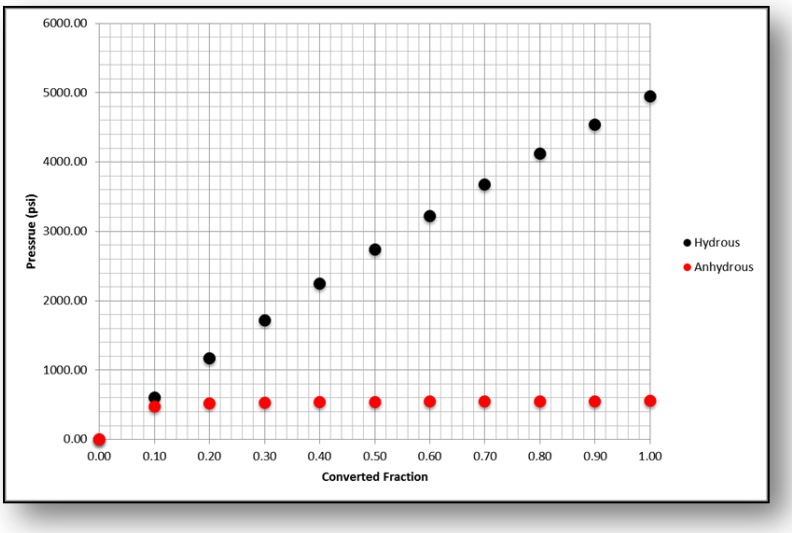

Figure 17: The role of water as a factor in pressure increase due to volume expansion.

For the role of organic richness, comparison between rich (25% TOC) and lean (3% TOC) is performed. Although the samples of (Lewan, 2011) experiment were 15.8 % TOC, two extremes in richness in the Green River Formation were intended to be used in the comparison. The factor is the water-to-kerogen volume ratio $\boldsymbol{V_R}$ and it is found to be:

$$\boldsymbol{V_R = \frac{V_{wi}[D_{kr} + a(TOC)(1-\phi)(1-D_{kr})]}{a(TOC)(1-\phi)\times 100}} \qquad (2)$$

$\boldsymbol{D_{kr}}$, $\boldsymbol{a}$, $\boldsymbol{\phi}$ are the kerogen to the rock density ratio, the transformation coefficient to organic matter (≈1.33) (Vernic, 1994), and matrix porosity (≈ 10%), respectively. By substituting back into equation (1), the difference in pressure increase for different organic richness can be observed (Figure 18). When 25% TOC is used to calculate the pressure increase, the volumetric ratio between water and kerogen is lowered. Consequently, the pressure significantly increased compared to a 3% TOC.

RICH
25% TOC

V_R	F	D_{ko}	C_w	C_o	C_k	C_o	Δ P
8.00	0.00	1.30	2.80E-08	3.00E-06	1.00E-05	1.50E-06	0.00
8.00	0.10	1.30	2.80E-08	3.00E-06	1.00E-05	1.50E-06	780.86
8.00	0.20	1.30	2.80E-08	3.00E-06	1.00E-05	1.50E-06	1514.62
8.00	0.30	1.30	2.80E-08	3.00E-06	1.00E-05	1.50E-06	2205.40
8.00	0.40	1.30	2.80E-08	3.00E-06	1.00E-05	1.50E-06	2856.87
8.00	0.50	1.30	2.80E-08	3.00E-06	1.00E-05	1.50E-06	3472.30
8.00	0.60	1.30	2.80E-08	3.00E-06	1.00E-05	1.50E-06	4054.60
8.00	0.70	1.30	2.80E-08	3.00E-06	1.00E-05	1.50E-06	4606.37
8.00	0.80	1.30	2.80E-08	3.00E-06	1.00E-05	1.50E-06	5129.96
8.00	0.90	1.30	2.80E-08	3.00E-06	1.00E-05	1.50E-06	5627.46
8.00	1.00	1.30	2.80E-08	3.00E-06	1.00E-05	1.50E-06	6100.78

LEAN
3% TOC

V_R	F	D_{ko}	C_w	C_o	C_k	C_o	Δ P
50.00	0.00	1.30	2.80E-08	3.00E-06	1.00E-05	1.50E-06	0.00
50.00	0.10	1.30	2.80E-08	3.00E-06	1.00E-05	1.50E-06	181.16
50.00	0.20	1.30	2.80E-08	3.00E-06	1.00E-05	1.50E-06	359.73
50.00	0.30	1.30	2.80E-08	3.00E-06	1.00E-05	1.50E-06	535.76
50.00	0.40	1.30	2.80E-08	3.00E-06	1.00E-05	1.50E-06	709.30
50.00	0.50	1.30	2.80E-08	3.00E-06	1.00E-05	1.50E-06	880.41
50.00	0.60	1.30	2.80E-08	3.00E-06	1.00E-05	1.50E-06	1049.13
50.00	0.70	1.30	2.80E-08	3.00E-06	1.00E-05	1.50E-06	1215.52
50.00	0.80	1.30	2.80E-08	3.00E-06	1.00E-05	1.50E-06	1379.63
50.00	0.90	1.30	2.80E-08	3.00E-06	1.00E-05	1.50E-06	1541.49
50.00	1.00	1.30	2.80E-08	3.00E-06	1.00E-05	1.50E-06	1701.16

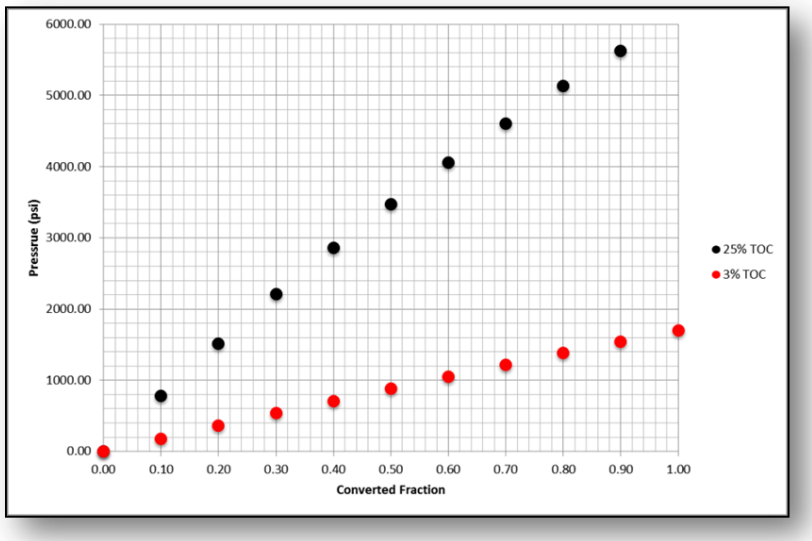

Figure 18: The role of organic richness in pressure increase.

Equation (1) can be written incorporating Young's modulus ($\boldsymbol{E}$) and Poisson's ratio ($\boldsymbol{v}$) to investigate the role of brittleness:

$$\boldsymbol{\Delta P = \frac{F(D_{ko}-1)}{V_R\left(\frac{3(1-2v)}{E}+C_w\right)+F(C_k+D_{ko}C_O)+\frac{3(1-2v)}{E}+C_w}} \qquad (3)$$

The effect of the brittleness in pressure increase is shown in Figure 19. A range of (2.5×10^6 to 1.0×10^7psi) is used for Young's modulus $\boldsymbol{E}$, and (0.1 to 0.26) is used for Poisson's ratio $\boldsymbol{\nu}$. High Young's modulus and low Poisson's ratio indicate high brittleness. High brittleness appears to generate higher pressure increase due to volume expansion.

BRITTLE

V_R	F	D_{ko}	C_w	E (psi)	ν	C_k	C_o	ΔP
11.80	0.00	1.30	2.80E-08	1.00E+07	0.10	1.00E-05	1.50E-06	0.00
11.80	0.10	1.30	2.80E-08	1.00E+07	0.10	1.00E-05	1.50E-06	2055.16
11.80	0.20	1.30	2.80E-08	1.00E+07	0.10	1.00E-05	1.50E-06	3799.30
11.80	0.30	1.30	2.80E-08	1.00E+07	0.10	1.00E-05	1.50E-06	5298.04
11.80	0.40	1.30	2.80E-08	1.00E+07	0.10	1.00E-05	1.50E-06	6599.79
11.80	0.50	1.30	2.80E-08	1.00E+07	0.10	1.00E-05	1.50E-06	7740.98
11.80	0.60	1.30	2.80E-08	1.00E+07	0.10	1.00E-05	1.50E-06	8749.59
11.80	0.70	1.30	2.80E-08	1.00E+07	0.10	1.00E-05	1.50E-06	9647.45
11.80	0.80	1.30	2.80E-08	1.00E+07	0.10	1.00E-05	1.50E-06	10451.87
11.80	0.90	1.30	2.80E-08	1.00E+07	0.10	1.00E-05	1.50E-06	11176.70
11.80	1.00	1.30	2.80E-08	1.00E+07	0.10	1.00E-05	1.50E-06	11833.20

DUCTILE

V_R	F	D_{ko}	C_w	E (psi)	ν	C_k	C_o	ΔP
11.80	0.00	1.30	2.80E-08	2.50E+06	0.26	1.00E-05	1.50E-06	0.00
11.80	0.10	1.30	2.80E-08	2.50E+06	0.26	1.00E-05	1.50E-06	1587.45
11.80	0.20	1.30	2.80E-08	2.50E+06	0.26	1.00E-05	1.50E-06	2986.08
11.80	0.30	1.30	2.80E-08	2.50E+06	0.26	1.00E-05	1.50E-06	4227.69
11.80	0.40	1.30	2.80E-08	2.50E+06	0.26	1.00E-05	1.50E-06	5337.32
11.80	0.50	1.30	2.80E-08	2.50E+06	0.26	1.00E-05	1.50E-06	6334.94
11.80	0.60	1.30	2.80E-08	2.50E+06	0.26	1.00E-05	1.50E-06	7236.70
11.80	0.70	1.30	2.80E-08	2.50E+06	0.26	1.00E-05	1.50E-06	8055.79
11.80	0.80	1.30	2.80E-08	2.50E+06	0.26	1.00E-05	1.50E-06	8803.08
11.80	0.90	1.30	2.80E-08	2.50E+06	0.26	1.00E-05	1.50E-06	9487.60
11.80	1.00	1.30	2.80E-08	2.50E+06	0.26	1.00E-05	1.50E-06	10116.95

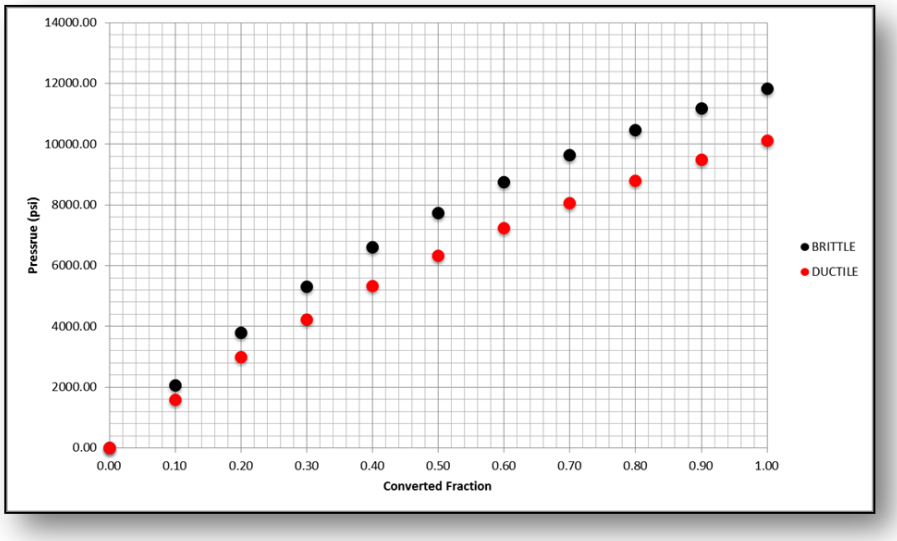

Figure 19: The role of brittleness in pressure increase.

<u>Microfracture initiation</u>:

Stress concentration around kerogen depends on its shape. Microfracture is initiated when the stress concentration is higher than the tensile strength of the rock:

$$-S_t > T \qquad (4)$$

The relationship between Oil-Yield and Total organic carbon (TOC) is utilized in this study for the purpose of determining the percentage of organic content (% Oc) and tensile strength. Oil-Yield has been defined by (Cook, 1974) for the Green River Formation:

$$\boldsymbol{Oil_{Yield}}\left(\boldsymbol{gallon\ per\ ton}\right) = 2.216\ (\%\boldsymbol{TOC}) - 0.7714 \quad (5)$$

In (Chong et.al., 1979) (% Oc) is defined as:

$$\left(\%\ \boldsymbol{Oc}\right) = \frac{\boldsymbol{157.76}(\boldsymbol{Oil_{Yield}})}{\boldsymbol{0.957}(\boldsymbol{Oil_{Yield}})+\boldsymbol{107}} \quad (6)$$

A study by (Dusseault et al., 1983) of mechanical properties of oil shales defines the tensile strength of the Mahogany zone of the Green River Formation as:

$$\boldsymbol{T} = 13.64 - 0.1211 \times (\%\ \boldsymbol{O_c}) \quad (7)$$

According to (Dusseault et al., 1983), the organic content is the property that primarily affects the results obtained in mechanical testing. The effects of varying quantities of other minerals such as dolomite on the strength and deformation properties of the Green River Formation are also important.

Considering a kerogen particle cross section projected along the principle (S_v) and the least (S_h) stresses plane (Figure 20). The kerogen is measured with an aspect ratio (ψ) having a width (w) and a height (h). At point x and y, the total stress concentration is equal to the internal concentration within the kerogen plus the external concentration outside the kerogen:

$$S_t = S_{out} + S_{in} \quad (8)$$

The aspect ratio (ψ) of the kerogen plays an important role in the initiation of the microfracture. For the minimum pressure increase to initiate horizontal microfracture, the following relationship is derived (Özkaya, 1988):

$$\Delta P > \frac{S_v(2-R)+T}{2\psi-1} \quad (9)$$

For initiating vertical microfracture, the minimum pressure increase to initiate vertical microfracture is:

$$\Delta P > \frac{RS_v+(^2/_\psi)S_v(R-1)+T}{\left(^2/_\psi-1\right)} \quad (10)$$

By comparing two different aspect ratios ($\psi = 3$ and $\psi = 1$), and considering a kerogen converted fraction between 20% to 30%, a microfracture will not be initiated when the aspect ratio is 1. Figure 21 shows the minimum pressure increase required to initiate a microfracture for both aspect ratios.

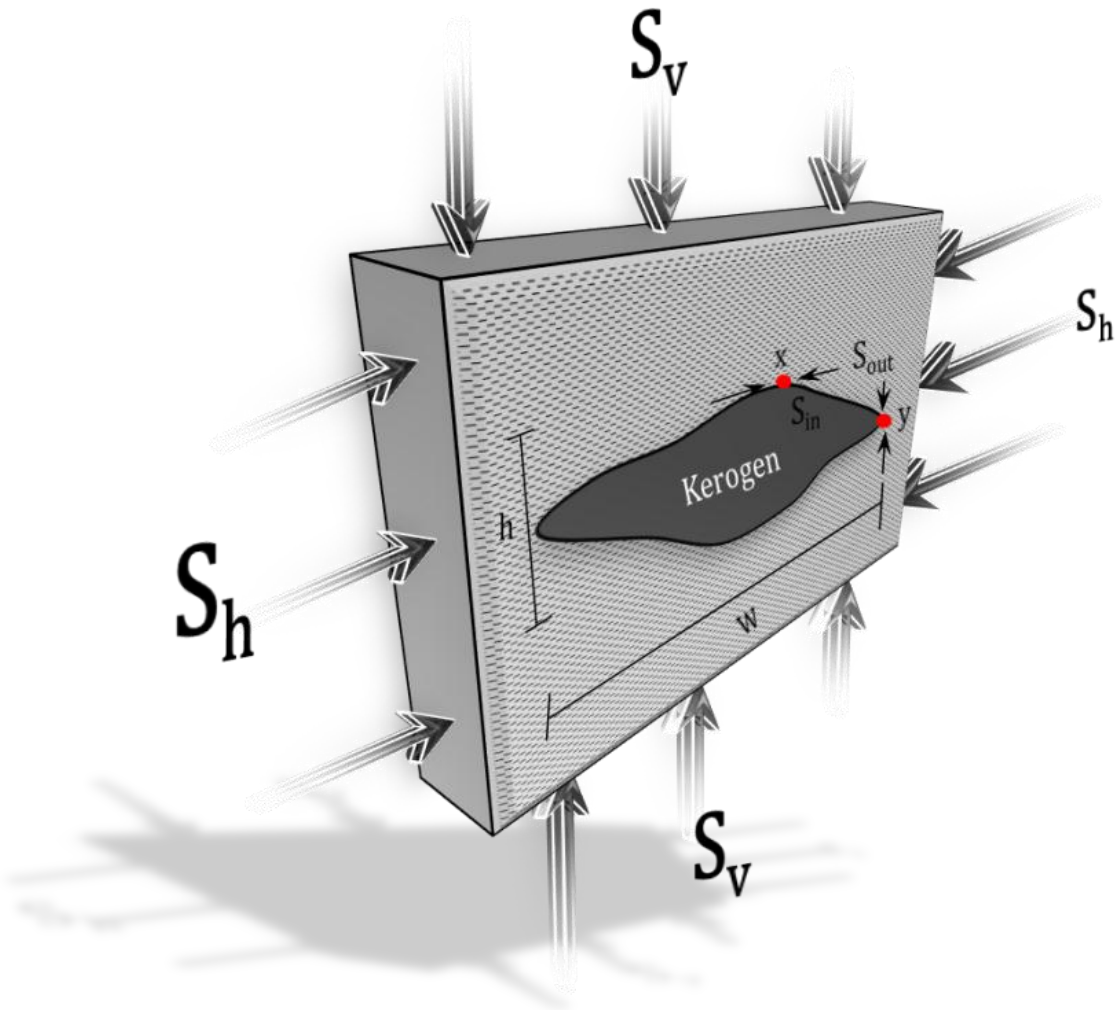

Figure 20: A section of a kerogen particle along (S_v) and (S_h) plane.

15.8% TOC							
V_R	F	D_{ko}	C_w	C_p	C_k	C_o	ΔP
11.80	0.00	1.30	2.80E-08	3.00E-06	1.00E-05	1.50E-06	0.00
11.80	0.10	1.30	2.80E-08	3.00E-06	1.00E-05	1.50E-06	600.90
11.80	0.20	1.30	2.80E-08	3.00E-06	1.00E-05	1.50E-06	1173.70
11.80	0.30	1.30	2.80E-08	3.00E-06	1.00E-05	1.50E-06	1720.33
11.80	0.40	1.30	2.80E-08	3.00E-06	1.00E-05	1.50E-06	2242.55
11.80	0.50	1.30	2.80E-08	3.00E-06	1.00E-05	1.50E-06	2741.96
11.80	0.60	1.30	2.80E-08	3.00E-06	1.00E-05	1.50E-06	3220.01
11.80	0.70	1.30	2.80E-08	3.00E-06	1.00E-05	1.50E-06	3678.05
11.80	0.80	1.30	2.80E-08	3.00E-06	1.00E-05	1.50E-06	4117.32
11.80	0.90	1.30	2.80E-08	3.00E-06	1.00E-05	1.50E-06	4538.93
11.80	1.00	1.30	2.80E-08	3.00E-06	1.00E-05	1.50E-06	4943.94

Favoring horizontal microfractures									
s_v	R	T	ψ >	ΔP	s_v	R	T	ψ >	ΔP
200	0.7	1350	3	322	200	0.7	1350	1	2013
200	0.7	1350	3	322	200	0.7	1350	1	2013
200	0.7	1350	3	322	200	0.7	1350	1	2013
200	0.7	1350	3	322	200	0.7	1350	1	2013
200	0.7	1350	3	322	200	0.7	1350	1	2013
200	0.7	1350	3	322	200	0.7	1350	1	2013
200	0.7	1350	3	322	200	0.7	1350	1	2013
200	0.7	1350	3	322	200	0.7	1350	1	2013
200	0.7	1350	3	322	200	0.7	1350	1	2013
200	0.7	1350	3	322	200	0.7	1350	1	2013
200	0.7	1350	3	322	200	0.7	1350	1	2013

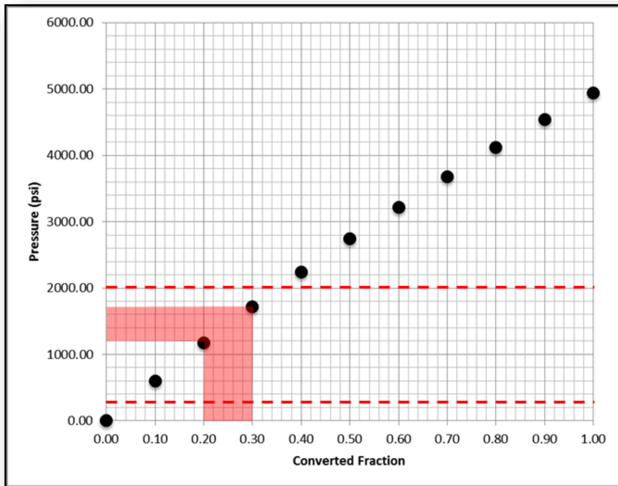

Figure 21: The role of aspect ratio in pressure increase. For aspect ratio of 3, the minimum pressure increase is 322 psi while a minimum of 2013 psi required for an aspect ratio of 1.

If the aspect ratio is large enough, higher chance for horizontal microfracturing. However, small aspect ratio favors vertical microfracturing (Figure 22 and 23).

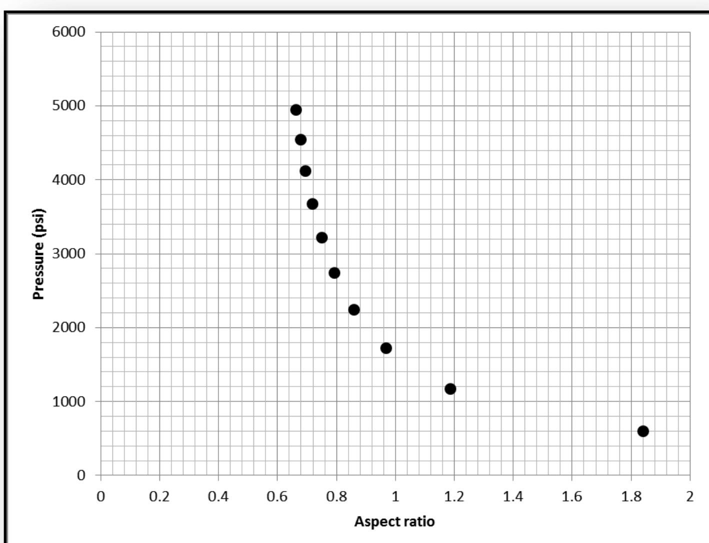

Figure 22: The minimum aspect ratio favoring horizontal microfracturing.

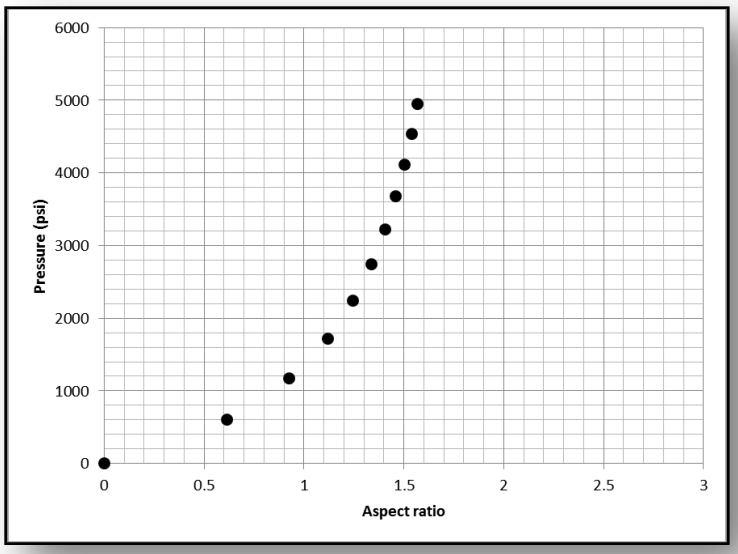

Figure 23: The maximum aspect ratio favoring vertical microfracturing.

Microfracture propagation:

The poroelastic behavior is expressed by (Engelder and Fischer, 1994):

$$S_h = \frac{\upsilon}{1-\upsilon}(S_v - \alpha P) + \alpha P \qquad (11)$$

Microfractures propagate vertically when the following conditions are true:

$$\kappa > 1$$

$$R \times \lambda < 1$$

Where $R = \frac{S_h}{S_v}$, $\lambda = \frac{\Delta P}{S_v}$, and $\kappa = \frac{\Delta P}{S_h}$

The poroelastic behavior favoring horizontal propagation is as follows:

$$R \times \lambda > 1$$

Figure 24 shows two examples of microfracture propagation (vertical and horizontal). Poisson's ratio and Biot coefficient are important factors controlling microfracture propagation. A set of different values are used and shown in figure 25, 26 and 27. Vertical propagation favors higher passion's ratio and lower Biot coefficient.

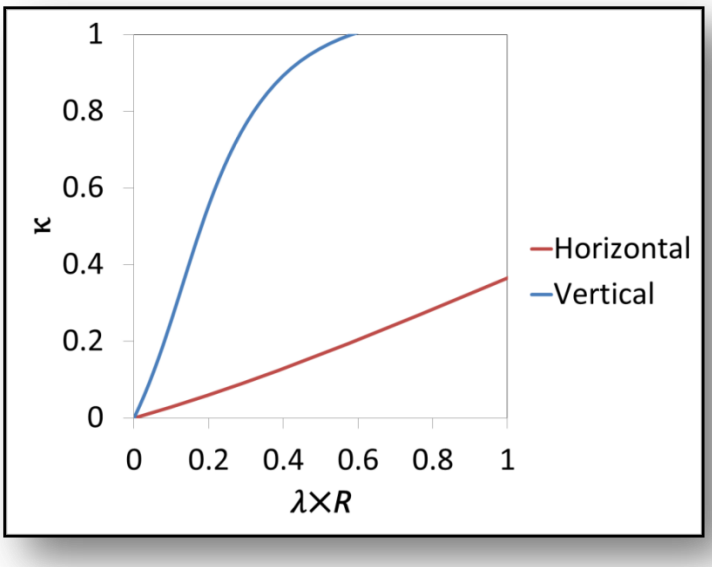

Figure 24: Vertical versus horizontal microfracture propagations

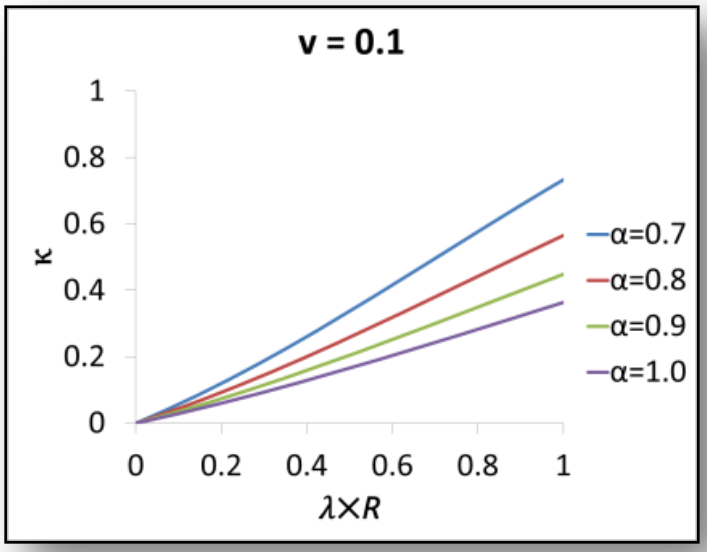

Figure 25: Poroelastic behavior for Poisson's ratio of 0.1 and different values for Biot coefficient.

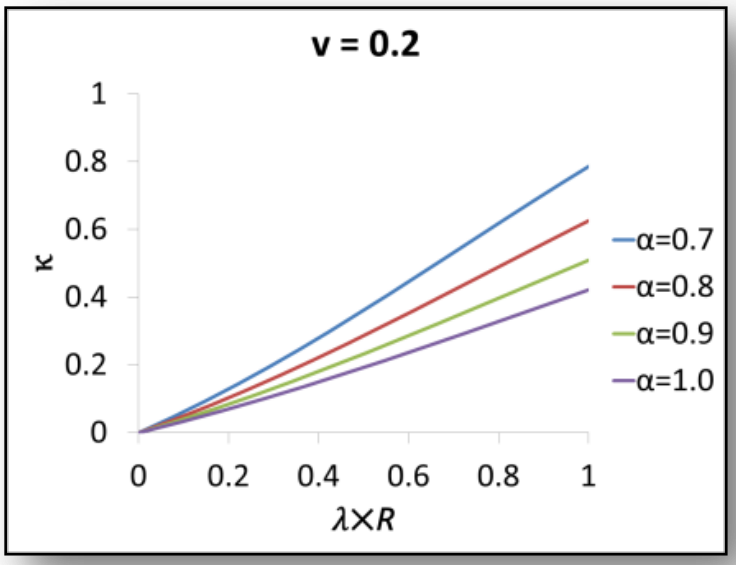

Figure 26: Poroelastic behavior for Poisson's ratio of 0.2 and different values for Biot coefficient.

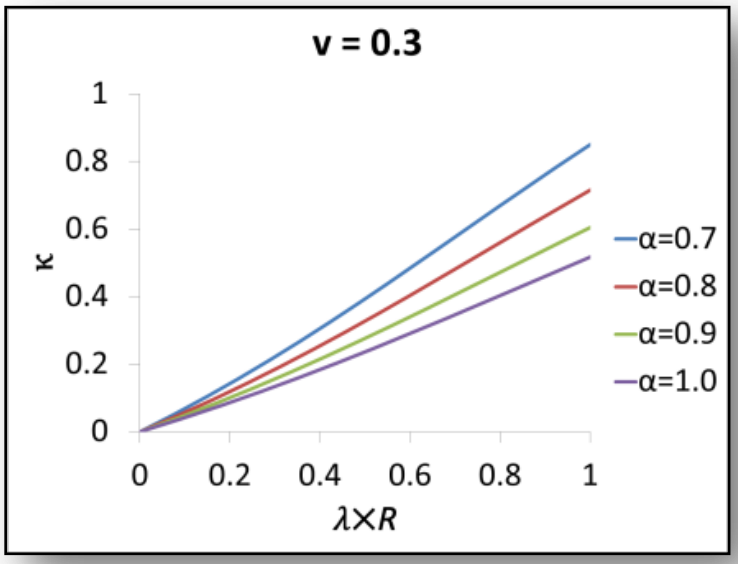

Figure 27: Poroelastic behavior for Poisson's ratio of 0.3 and different values for Biot coefficient.

CONCLUSIONS AND RECOMMENDATIONS

The significance of microfractures resides in its ability to provide higher permeability pathways through organic-rich shales that may explain their high deliverability. The volume expansion due to hydrocarbon generation has been invoked as a mechanism to increase pressures to the level of inducing bedding-parallel microfractures responsible for primary migration of oil from kerogen. The process of microfracturing in organic-rich shales due to hydrocarbon generation involves four stages: 1) volume expansion, 2) pressure increase, 3) microfracture initiation, 4) microfracture propagation.

Despite the widespread observed evidence for the existence of hydrocarbon-generation microfracturing, a comprehensive description of this phenomenon has proven to be extraordinarily difficult to develop. However, As a result of an understanding which currently is evolving concerning the factors controlling volume expansion, pressure increase, initiation and propagation of microfractures, it appears that the existence of water, the level of richness and brittleness play a major role in controlling pressure increase due to volume expansion.

The geometric shape of the kerogen controls hydrocarbon-generation microfracturing. High aspect ratio which indicate thin flakes of kerogen favor horizontal microfracturing. If the aspect ratio is not high enough, vertical microfracturing is favored.

The in-situ stress state completely governs the propagation of microfractures. There is no vertical stress constrain on the experiment done on the Green River Formation samples. This will cause horizontal microfracturing without the need to have higher pressures to overcome the principle vertical stress and create the observed horizontal microfractures. It is recommended to preform similar pyrolysis experiment using different conditions with different vertical stress applied. This will enable to have more robust analysis for microfracture prorogation.

As shown in Figure 28, the hydrocarbon-generation microfracturing follows a sequence of:

1. Thermal maturation of organic-rich shale
2. Conversion of kerogen to bitumen
3. Creation of kerogen nanoporosity
4. Conversion of bitumen to oil
5. Significant expansion of hydrocarbon volume and increase in pressure
6. Controlled initiation of microfractures by kerogen aspect ratio
7. Controlled propagation of microfractures by poroelastic behavior

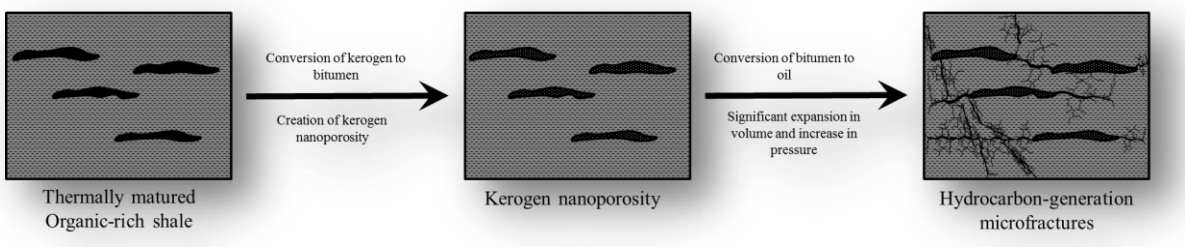

REFERENCES

Berg, R. R., and A. F. Gangi 1999, Primary migration by oil-generation microfracturing in low-permeability source rocks: application to the Austin Chalk, Texas, AAPG Bull., 83, 727– 756.

Chalmers, G.R.L., and R.M. Bustin., 2007, The organic matter distribution and methane capacity of the Lower Cretaceous strata of northeastern British Columbia, Canada: International Journal of Coal Geology, v. 70, p. 223–239.

Chong, K.P., J. Ward, and B. Chang, 1979. Oil Shale Properties by Split Cylinder Method. J. Geotech. Engn. Div. ASCE, Vol. 105, Ngt. 5, P 595-611,(l)

Cluff, R. M., K. W. Shanley, and M. A. Miller, 2007, Three things we thought we understood about shale gas, but were afraid to ask, AAPG Search and Discover Article #90063, AAPG Annual Convention, Long Beach, California.

Cook, E. W., 1974, Green River Shale-oil yields: correlation with elemental analysis, FUEL, v. 53.

Dusseault, M.B, K. L. Bradshaw, K. Ehret, and M. Loftsson, 1983, The Mechanical Properties of oil Shales, Ontario Geological Survey Open File Report.

Dusseault, M. B and M. Loftsson,1985, The Mechanical Properties of the Kettle Point Oil Shale, Ontario Geological Survey Open File Report 5560, 93p.

Engelder T and Lacazette A, 1990, Natural Hydraulic Fractures. In Barton, N. and Stephanson, O, eds, Rock Joints, Rotterdam, A. A. Balkema, 35-44.

Fouch, T. D., D. D. Rice, V. F. Nuccio, J. K. Pitman, D. E. Anders, R. F. Mast, 1994, Green River(!) Petroleum System, Uinta Basin, Utah, U.S.A., in Magoon, L. B, and W. G. Dow, eds., 1994, The Petroleum System—from source to trap: AAPG Memoir 60

Jarvie, D.M., R.J., Hill, T.E. Ruble, and R.M. Pollastro, 2007, Unconventional shale-gas systems: the Mississippian Barnett Shale of north central Texas as one model for thermogenic shale-gas assessment, in Hill, R.J., and Jarvie, D.M., eds., Special Issues: Barnett Shale, American Association of Petroleum Geologists, Bulletin, v. 91, p. 475–499.

Johnson, R.C., Mercier, T.J., Ryder, R.T., Brownfield, M.E., and Self, J.G., 2011, Assessment of in-place oil shale resources of the Eocene Green River Formation, Greater Green River Basin, Wyoming, Colorado, and Utah, in U.S. Geological Survey Oil Shale Assessment Team, ed., Oil shale resources of the Eocene Green River Formation, Greater Green River Basin, Wyoming, Colorado, and Utah: U.S. Geological Survey Digital Data Series DDS–69–DD, chap. 1, 63 p., 1 plate.

Lash, G. G., and T. Engelder, 2005, An analysis of horizontal microcracking during catagenesis: Example from the Catskill delta complex, AAPG Bulletin, 89, pp. 1433– 1449.

Lewan M. D., 1985, Evaluation of petroleum generation by hydrous pyrolysis experimentation. Phil. Trans. Roy. Soc. London 315, 123- 134.

Lewan M. D., 1987, Petrographic study of primary petroleum migration in the Woodford shale and related rock units. In Migration of Hydrocarbons in Sedimentary Basins (ed. B. Doligez), pp. 113-130. Editions Technip.

Lewan, M. D. and S. Roy, 2011, Role of water in hydrocarbon generation from type-1 Kerogen in Mahogany oil shale of the Green River Formation, Organic Geochemistry 42, pp. 31-41.

Loucks, R. G., R. M. Reed, S. C. Ruppel, and D. M. Jarvie, 2009, Morphology, Genesis, and Distribution of Nanometer-Scale Pores in Siliceous Mudstones of the Mississippian Barnett Shale, Journal of Sedimentary Research, v. 79, pp. 848-861

Meissner, F. F., 1978b, Petroleum geology of the Bakken Formation, Williston Basin, North Dakota and Montana, in 24th Annual conference, Williston Basin symposium: Montana Geological Society, p. 207–227.

Momper, J. A., 1978, Oil migration limitations suggested by geological and geochemical considerations, AAPG Continuing Education Course Note Series 8, pp. B1-B60.

O'Brien, N. R., G. D. Thyne, and R. M. Slatt, 1996, Morphology of Hydrocarbon Droplets During Migration: Visual Example from the Monterey Formation (Miocene), California.

Özkaya, I., 1988, A simple analysis of oil-induced fracturing in sedimentary rocks, Marine and Petroleum Geology, v. 5, pp. 293–297.

Rickman, R., M. Mullen, E. Petre, B. Grieser, D. Kundert, 2008, A practical Use of Shale Petrophysics for Stimulation Design Optimization: All Shale Plays Are Not Clones of the Barnett Shale, SPE 115258, SPE Annual Technical Conference and Exhibition, Denver, Colorado, USA.

Ruble, T. E., M. D. Lewan, and R. P. Philp, 2001, New Insights on the Green River Petroleum System in the Uinta Basin from Hydrous Pyrolysis Experiments, AAPG Bulletin, v. 85, no. 8, pp. 1333-1371.

Secor, D. T., 1965, Role of fluid pressure in jointing, American Journal of Science 263, pp. 633-646.

Swarbrick, R.E. and M.J. Osborne, 1998, Mechanisms that generate abnormal pressures: an overview, in Law, B.E., G.F. Ulmishek, and V.I. Slavin eds., Abnormal pressures in hydrocarbon environments: AAPG Memoir 70, p. 13–34.

Wren, A. E., 2011, The Prospectivity of Unconventional Oil and Gas Resources in the Vaca Muerta Shale of the Neuquen Basin of Argentina, paper presented at the World Shale Gas Conference and Exhibition, Houston, USA.

Vanden Berg, M. D., 2008, Basin-Wide Evaluation of the Uppermost Green River Formation's Oil-Shale Resource, Uinta Basin, Utah and Colorado, Special study 128, Utah Geological Survey

Vernic, L., 1994, Hydrocarbon-generation-induced microcracking of source rocks, GEOPHYSICS, v. 59, no. 4, pp. 555-563

APPENDIX

Volume Expansion Equations (Berg, 1999):

Before HC generation: $\boldsymbol{V_P(P_i) = V_{P_i} = V_{wi} + V_{ki}}$

After HC generation: $\boldsymbol{V_P(P) = V_P = V_w + V_k + V_o}$

$V_P(P_i) = V_{P_i} = Pore\ volume\ at\ initial\ pressure, before\ hydrocarbon\ generation$
$V_P(P) = V_P = Pore\ volume\ at\ increased\ pressure, after\ hydrocarbon\ generation$
$V_{wi} = Volumetric\ water\ content\ before\ hydrocarbon\ generation$
$V_w = Volumetric\ water\ content\ after\ hydrocarbon\ generation$
$V_{ki} = Volumetric\ Kerogen\ content\ before\ hydrocarbon\ generation$
$V_k = Volumetric\ Kerogen\ content\ after\ hydrocarbon\ generation$
$V_o = Volumetric\ hydrocarbon\ content\ generated$

Mass Balance Approach:

$\boldsymbol{V_P(P_i) = V_P(P)}$

$\boldsymbol{V_{P_i} = V_P}$

$\boldsymbol{V_w = V_{wi}}$ (No water loss)

$\boldsymbol{V_k = V_{ki} - FV_{ki}}$

$\boldsymbol{V_o = F\left(\frac{\rho_k}{\rho_o}\right)V_{ki}}$ $\boldsymbol{\left(\frac{\rho_k}{\rho_o} = D_{ko}\right)}$

$F = Converted\ fraction\ of\ Kerogen$

$\rho_k = Density\ of\ Kerogen$
$\rho_o = Density\ of\ Oil$
$D_{ko} = Kerogen - Oil\ density\ ratio$

Compressibility and relationship with volume and pressure:

$$\boldsymbol{C_P = +\frac{1}{V}\frac{\partial V}{\partial P_i}}$$
$$\boldsymbol{V_P(P_i) = V_{P_i}(1 + C_P \Delta P)}$$
$$\boldsymbol{= (V_{wi} + V_{ki})(1 + C_P \Delta P)}$$

$$\boldsymbol{C_{w,k,o} = -\frac{1}{V}\frac{\partial V}{\partial P}}$$
$$\boldsymbol{V_P(P) = V_{w,k,o}\left(1 - C_{w,k,o}\Delta P\right)}$$

Solving for ΔP using mass balance approach:

$$\boldsymbol{V_{P_i} = V_P}$$

$$\boldsymbol{(V_{wi} + V_{ki})(1 + C_P \Delta P) = V_{wi}(1 - C_w \Delta P) + V_{ki}(1 - C_k \Delta P) - FV_{ki}(1 - C_k \Delta P) + FD_{ko}V_{ki}(1 - C_o \Delta P)}$$

Expand:

$$\boldsymbol{V_{wi} + V_{wi}C_P\Delta P + V_{ki} + V_{ki}C_P\Delta P}$$
$$\boldsymbol{= V_{wi} + V_{wi}C_w\Delta P + V_{ki} - V_{ki}C_k\Delta P - FV_{ki} - FV_{ki}C_k\Delta P + FD_{ko}V_{ki} - FD_{ko}V_{ki}C_o\Delta P}$$

Rearranging and dividing by $\boldsymbol{V_{ki}}$:

$$\boldsymbol{\left(\frac{V_{wi}}{V_{ki}}\right)C_P\Delta P + C_P\Delta P + \left(\frac{V_{wi}}{V_{ki}}\right)C_w\Delta P + C_k\Delta P + FC_k\Delta P + FD_{ko}C_O\Delta P = F(D_{ko} - 1)}$$

$$\boldsymbol{\Delta P\left(\left(\frac{V_{wi}}{V_{ki}}\right)C_P + C_P + \left(\frac{V_{wi}}{V_{ki}}\right)C_w + C_k + FC_k + FD_{ko}C_O\right) = F(D_{ko} - 1)}$$

$\left(\frac{V_{wi}}{V_{ki}}\right) = V_R$

$$\boldsymbol{\Delta P = \frac{F(D_{ko} - 1)}{V_R(C_P + C_w) + F(C_k + D_{ko}C_O) + C_P + C_w}}$$

Volumetric Kerogen content in terms of TOC and porosity:

Vernic (1994):

$$\boldsymbol{V_{ki} = \frac{a(TOC)(1-\phi)\rho_m}{\rho_k + a(TOC)(1-\phi)(\rho_m - \rho_k)}}$$

Dividing by $\boldsymbol{\rho_m}$:

$$\boldsymbol{V_{ki} = \frac{a(TOC)(1-\phi)}{D_{kr} + a(TOC)(1-\phi)(1-D_{kr})} \times 100}$$

Substituting into V_R

$$\boldsymbol{V_R = \frac{V_{wi}[D_{kr} + a(TOC)(1-\phi)(1-D_{kr})]}{a(TOC)(1-\phi) \times 100}}$$

$a = transformation\ coefficient\ to\ organic\ matter \approx 1.33$
$\rho_m = matrix\ density$
$\phi = matrix\ porosity$
$D_{kr} = Kerogen - rock\ density$

Brittleness effect in pressure increase:

(Rickman et.al., 2008)

$$\mathbf{B} = \frac{\boldsymbol{E_B + v_B}}{\mathbf{2}}$$

$$\boldsymbol{E_B = \left(\frac{E-1}{8-1}\right) \times 100}$$

$$\boldsymbol{v_B = \left(\frac{v - 0.4}{0.15 - 0.4}\right) \times 100}$$

Brittleness can be calculated separately to avoid making a complicated term.

High Young's' modulus, Low Poisson's ratio ⟶ more brittleness

$$\boldsymbol{C_P = \frac{1}{K}}$$

$$\boldsymbol{K = \frac{E}{3(1-2v)}}$$

$$\boldsymbol{C_P = \frac{3(1-2v)}{E}}$$

Substituting back into ΔP:

$$\boldsymbol{\Delta P = \frac{F(D_{ko}-1)}{V_R\left(\frac{3(1-2v)}{E}+C_w\right)+F(C_k+D_{ko}C_O)+\frac{3(1-2v)}{E}+C_w}}$$

$K = Bulk\ modulus$
$E = Young's\ modulus$
$v = Poisson's\ ratio$
$B = Brittleness$

Pressure increase and principle stresses:

$$P = S_v + \Delta P$$

$$R = \frac{S_h}{S_v}$$

$P = \ pressure$
$\Delta P = Pressure\ increase$
$S_v = Total\ vertical\ stress$
$S_h = Total\ minimum\ horizontal\ stress$
$R = Total\ minimum\ horizontal\ stress\ to\ vertical\ stress\ ratio$

Conditions for initiation of microfractures:

Modified from (Özkaya, 1987) this is modified from (Jaeger and Cook, 1976)

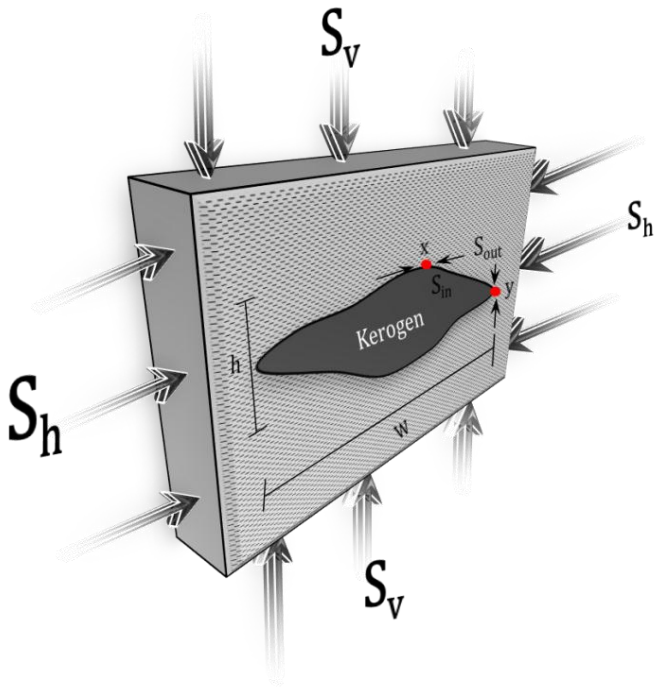

Tangential stress at x, y due to S_v and S_h:

At x: $S_{out} = S_h\left(1 + {}^{2}/_{\psi}\right) - S_v$

At y: $S_{out} = S_v(1 + 2\psi) - S_h$

Tangential stress at x, y due to internal stress S_{in} that is due to Pressure P:

At x: $S_{in} = P\left(1 - {}^{2}/_{\psi}\right)$

At y: $S_{in} = P(1 - 2\psi)$

Total tangential stress at x and y:

$S_t = S_{out} + S_{in}$

$S_{t_x} = S_h\left(1 + {}^{2}/_{\psi}\right) - S_v + P\left(1 - {}^{2}/_{\psi}\right)$

$S_{t_y} = S_v(1 + 2\psi) - S_h + P(1 - 2\psi)$

Initiation of microfracture:

$-S_t > T$

Favoring horizontal microfracturing:

$-S_{t_y} > T$

$-S_v(1 + 2\psi) + S_h - P(1 - 2\psi) > T$

$P(2\psi - 1) > S_v(1 + 2\psi) - S_h + T$

From $(P = S_v + \Delta P)$ *and* $\left(R = \frac{S_h}{S_v}\right)$

$(S_v + \Delta P)(2\psi - 1) > S_v(1 + 2\psi) - RS_v + T$

Rearranging:

$\Delta P(2\psi - 1) > 2S_v - RS_v + T$

For minimum pressure increase to initiate horizontal microfracture:

$$\Delta P > \frac{S_v(2-R)+T}{2\psi-1}$$

For minimum aspect ratio to initiate horizontal microfracture:

$$\psi > \frac{1}{2} + \frac{S_v(2-R)+T}{2\Delta P}$$

$$\psi = \frac{w}{h}$$

Favoring vertical microfracturing:

$$-S_{t_x} > T$$

$$-S_h\left(1+{}^{2}/_{\psi}\right) + S_v - P\left(1-{}^{2}/_{\psi}\right) > T$$

$$P\left({}^{2}/_{\psi}-1\right) > S_h\left(1+{}^{2}/_{\psi}\right) - S_v + T$$

From $(P = S_v + \Delta P)$ *and* $\left(R = \frac{S_h}{S_v}\right)$

$$(S_v + \Delta P)\left({}^{2}/_{\psi}-1\right) > RS_v\left(1+{}^{2}/_{\psi}\right) - S_v + T$$

Rearranging:

$$\Delta P\left({}^{2}/_{\psi}-1\right) > RS_v + ({}^{2}/_{\psi})S_v(R-1) + T$$

For minimum pressure increase to initiate vertical microfracture:

$$\Delta P > \frac{RS_v + ({}^{2}/_{\psi})S_v(R-1)+T}{\left({}^{2}/_{\psi}-1\right)}$$

For minimum aspect ratio to initiate vertical microfracture:

$$\psi < \frac{2\Delta P}{RS_v + \left({}^{2}/_{\psi}\right)S_v(R-1)+T+\Delta P}$$

Poroelastic behavior is expressed (Engelder and Fischer, 1994):

$$S_h = \frac{\upsilon}{1-\upsilon}(S_v - \alpha P) + \alpha P$$

$$R = \frac{S_h}{S_v}$$

$$\lambda = \frac{\Delta P}{S_v}$$

$$\kappa = \frac{\Delta P}{S_h}$$

$$\alpha = Biot\ poroelastic\ coefficient$$

Poroelastic behavior favoring vertical propagation:

$$\kappa > 1$$

$$R \times \lambda < 1$$

Poroelastic behavior favoring horizontal propagation:

$$R \times \lambda > 1$$